Age-related dopaminergic innervation augments T helper 2-type allergic inflammation in the postnatal lung

Wei Wang[1], Jonathan A. Cohen[1], Antonia Wallrapp[2], Kenneth G. Trieu[1], Juliana Barrios[3], Fengzhi Shao[3], Nandini Krishnamoorthy[1], Vijay K. Kuchroo[2], Matthew R. Jones[3], Alan Fine[3,4], Yan Bai[1], Xingbin Ai[1,5,*,¶]

[1]Division of Pulmonary and Critical Care Medicine, Department of Medicine, Brigham and Women's Hospital, Boston, Massachusetts, USA

[2]Evergrande Center for Immunologic Diseases, Harvard Medical School and Brigham and Women's Hospital, Boston, Massachusetts, USA

[3]The Pulmonary Center, Department of Medicine, Boston University School of Medicine, Boston, Massachusetts, USA

[4]The West Roxbury Veteran's Hospital, West Roxbury, Massachusetts, USA

[5]Lead contact

Abstract

Young children are more susceptible to developing allergic asthma than adults. As neural innervation of the peripheral tissue continues to develop after birth, neurons may modulate tissue inflammation in an age-related manner. Here, we showed that sympathetic nerves underwent a dopaminergic-to-adrenergic transition during postnatal development of the lung in mice and humans. Dopamine signaled through a specific dopamine receptor (DRD4) to promote T-helper 2 (Th2) cell differentiation. The dopamine-DRD4 pathway acted synergistically with the cytokine IL-4 by upregulating IL-2-STAT5 signaling and reducing inhibitory histone trimethylation at Th2 gene loci. In murine models of allergen exposure, the dopamine-DRD4 pathway augmented Th2 inflammation in the lung of young mice. However, this pathway marginally operated after sympathetic nerves became adrenergic in the adult lung. Taken together, the communication

[*]Correspondence: Xingbin Ai, Division of Pulmonary and Critical Care Medicine, Department of Medicine, Brigham and Women's Hospital, Boston, Massachusetts, USA. Phone: 617-732-5218; xai@partners.org.
[¶]Current address: Division of Newborn Medicine, Department of Pediatrics, Massachusetts General Hospital for Children, Boston, Massachusetts, USA.

Conflict of interest: The authors have declared that no conflict of interest exists.

Declaration of interests
The authors declare no competing interests.

between dopaminergic nerves and CD4^{+} T cells provides an age-related mechanism underlying the susceptibility to allergic inflammation in the early lung.

Graphical Abstract
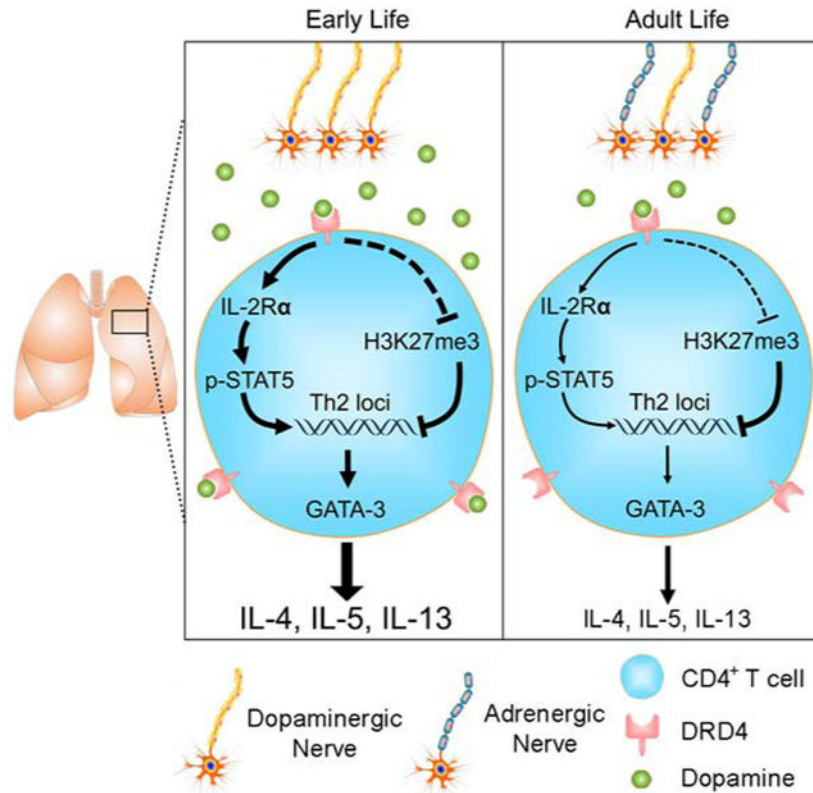
eTOC blurb

Children are more prone to develop allergic asthma than adults. Wang et al. find that sympathetic nerves undergo a dopaminergic-to-adrenergic transition during postnatal development of the lung. Dopamine signaling in CD4^{+} T cells promotes a Th2 phenotype, which makes young mice more susceptible to allergy. These findings provide an age-related mechanism underlying the susceptibility of the young to allergic inflammation.

Keywords

allergic asthma; Th2; sympathetic nerve; dopamine; DRD4; IL-2; IL-4

Introduction

The nervous system communicates with the immune system to regulate inflammation. Pathogen exposure and tissue injury stimulate immune cells and trigger a neural reflex (Chavan et al., 2017). The activation of the neural reflex causes the release of neurotransmitters from the innervating afferent and efferent neurons. These neurotransmitters can signal to immune cells thereby modulating innate and adaptive

immune responses. For example, the cholinergic vagal system is activated in sepsis and by releasing acetylcholine, represses tumor necrosis factor production in spleen macrophages (Borovikova et al., 2000; Wang et al., 2003). In other organs, such as the gut, cholinergic and sympathetic nerves play opposing roles in modulating innate lymphoid type 2 cell (ILC2)-mediated type 2 inflammation by secreting neuromedin U and epinephrine, respectively (Cardoso et al., 2017; Klose et al., 2017; Moriyama et al., 2018).

Allergic asthma is a common airway disease characterized by eosinophilia, mucus overproduction, airway hyperreactivity and tissue remodeling (Becerra-Diaz et al., 2017; Fahy, 2015). These hallmarks are driven by type 2 cytokines including IL-4, IL-5 and IL-13. A major effector cell in asthma is T helper 2 (Th2) cells. These cells are differentiated from naive $CD4^+$ T cells through a well-orchestrated process that involves priming in the lymph node and maturation in the lung (Van Dyken et al., 2016). Th2 cell differentiation requires IL-4 and IL-2. IL-4 induces differentiation and maintains the Th2 phenotype (Le Gros et al., 1990), while IL-2, which is expressed by T cells upon activation, promotes proliferation and Th2 differentiation by transcriptionally activating the expression of *Il2ra, Il4* and *Il4ra* genes via STAT5 (Cote-Sierra et al., 2004; Zhu et al., 2003). Apart from cytokines, neurotransmitters modulate type 2 inflammation. Neuropeptides are known to enhance the antigen-presenting activity of dendritic cells in adult murine models of allergic asthma (Buttari et al., 2014; Ohtake et al., 2015; Talbot et al., 2015). Dopamine has also been shown to induce a Th2 phenotype in $CD4^+$ T cells in culture (Huang et al., 2010; Nakano et al., 2009). However, the intracellular signaling mechanism of dopamine driving Th2 cell differentiation is unknown. In addition, there are conflicting reports of the identity of the dopamine receptors involved and the role of dopamine in disease models (Contreras et al., 2016; Franz et al., 2015; Huang et al., 2010; Ilani et al., 2004; Mori et al., 2013; Nakano et al., 2009).

To date, the studies related to neural regulation of type 2 inflammation have been limited to mature tissues in adult disease models. As neurons undergo dynamic changes in the abundance and phenotype during postnatal maturation, the neuron-immune cell communication may differ with age thereby contributing to disease susceptibility in a tissue-specific and age-related manner. This age-related communication may be particularly important to asthma, as young children are more susceptible to develop allergic asthma than adults (Stern et al., 2008).

In the lung, nerves innervate the smooth muscle compartment in the airway and vasculature. These nerves are mostly derived from neurons whose cell bodies are located outside of the pulmonary tract in the nodose ganglion, sympathetic ganglion and brain stem. Nodose sensory afferents and cholinergic and sympathetic efferents are connected through the brain stem neurons to form a neurocircuitry that controls fundamental respiratory functions, such as breathing and cough (Aven and Ai, 2013). The development of the neurocircuitry requires locally produced neurotrophins, such as brain-derived neurotrophic factor and neurotrophin 4 (Aven et al., 2014; Patel et al., 2016; Radzikinas et al., 2011). The temporal expression of these neurotrophins dynamically regulates the process of airway innervation during embryogenesis and postnatal maturation. In the murine lung, neural innervation peaks

around postnatal day 14 (P14) followed by a decline in the third postnatal week before it reaches the mature configuration in adults (Aven et al., 2014).

In this study, we characterized the postnatal development of the 3 major types of nerves in the murine lung and discovered that sympathetic nerves transitioned from a predominantly dopamine-producing (dopaminergic) phenotype in early postnatal life to a norepinephrine-producing (adrenergic) phenotype in adult life. We investigated dopamine signaling in T cells and in murine models of allergic inflammation. We found that dopaminergic nerves in the early lung augmented Th2 inflammation by communicating with CD4$^+$ T cells via the dopamine-DRD4 pathway, while adrenergic nerves in the adult lung had no Th2-inducing activities. Our findings provide evidence for the development of sympathetic innervation as an age-related modulatory mechanism in Th2 inflammation in the lung, which has implications for the susceptibility and etiology of allergic asthma in young children.

Results

Sympathetic nerves in the lung undergo a dopaminergic-to-adrenergic transition during postnatal development.

We characterized the developmental dynamics of the 3 major types of nerves in murine lung after birth. Western blot analysis showed that the relative abundance of sensory and cholinergic nerves, identified by calcitonin gene-related peptide (CGRP) and vesicular acetylcholine transporter (VAChT) respectively, remained mostly unchanged by age (Figure 1A). For sympathetic nerves, however, tyrosine hydroxylase (TH), which is a specific marker and the rate-limiting enzyme for the biosynthesis of dopamine, peaked around postnatal day 15 (P15)-P21 followed by a decline in the adult lung, while the amount of dopamine β-hydroxylase (DBH), an enzyme that converts dopamine to norepinephrine, increased with age (Figures 1A and 1B). These changes in tyrosine hydroxylase and DBH were associated with a 50% reduction in the amount of dopamine from P21 (961.9 ± 66.72 pg/mg lung weight) to adults (494.0 ± 114.7 pg/mg lung weight) with a reciprocal increase in norepinephrine (1815 ± 349 pg/mg lung weight at P21 versus 3469 ± 669 pg/mg lung weight in adults) (Figure 1C).

Previous studies detected tyrosine hydroxylase in a subset of immune cells mostly by gene expression assays (Cosentino et al., 2007; Flierl et al., 2007; Papa et al., 2017). To address whether the age-related reduction in tyrosine hydroxylase expression in the postnatal lung was caused by a change in sympathetic innervation, we investigated the source of tyrosine hydroxylase in both mouse and human lungs. Because the lung sample in Western blot and dopamine measurement assays likely included lymph nodes associated with bronchi, we separately examined the lung and associated lymph nodes. Due to technical difficulties of dissecting lymph nodes associated with mouse lungs especially in neonates, we resorted to lymph nodes associated with human donor lungs for the assay. Double staining for tyrosine hydroxylase and a pan-neural marker, neuron-specific class III β-tubulin (TUBB3) detected tyrosine hydroxylase exclusively in TUBB3$^+$ structures along the airway and blood vessel in mice and humans (Figures 1D and 1F). In addition, tyrosine hydroxylase and DBH were found selectively in nerves along the lymphatic vessel in lymph nodes associated with adult donor lungs (Figures 1H and S1A). DBH was also found only in nerves in the mouse lung

(Figure S1B). Furthermore, tyrosine hydroxylase in isolated mouse splenocytes and purified CD4$^+$ T cells was below detection compared to robust expression in neurons (Figure 1J).

After validating the nerve as the major source of tyrosine hydroxylase, we quantified the abundance of sympathetic nerves in immature and adult lungs. To control for variations caused by the size of the airway, we normalized the immunoreactivity of tyrosine hydroxylase to TUBB3. We found the extent of tyrosine hydroxylase$^+$ innervation was a fold higher in P19 mice and children (0-13 years of age) compared to the adult counterparts (3-4 months of age in mice and 40-65 years of age in humans) (Figures 1E and 1G). In addition, lymph nodes associated with donor lungs had more abundant tyrosine hydroxylase but less DBH in children compared to adults by Western blot and antibody staining (Figures 1I and S1A). Taken together, sympathetic nerves that innervate the lung and associated lymph nodes transition from a predominantly dopaminergic phenotype in early postnatal life to an adrenergic phenotype in adulthood. In accordance, the sympathetic nerve system in the adult lung is known to be mostly adrenergic (Felten et al., 1985).

Dopamine promotes a Th2 phenotype of naïve CD4$^+$ T cells.

We tested whether sympathetic nerves played an age-related role in inflammation by releasing dopamine in the early lung. Dopamine was previously shown to induce Th2 cytokine expression *in vitro* (Huang et al., 2010; Nakano et al., 2009). To investigate the mechanism of dopamine signaling in Th2 cell differentiation, we isolated naïve CD4$^+$ T cells from mouse spleen using a negative selection kit. Cells were stimulated with αCD3 and αCD28 alone (Th0) and in the presence of IL-4 (Th0+IL-4). Dopamine dose-dependently elevated the expression of IL-4, IL-5 and IL-13 in Th0 cultures (Figure 2A). In contrast, norepinephrine and epinephrine, two neurotransmitters that are enzymatically converted from dopamine, had no Th2-inducing activities (Figures S1E and S1F). The activity of dopamine peaked at 10 μM by doubling the amount of Th2 cytokines in Th0 and Th0+IL-4 cultures at day 4 (Figures 2A-2C and S1C), while repressing Th1 cytokines, such as *Ifng* (Figure S1D). We thus used 10 μM dopamine for all *in vitro* studies. We noted that the extent of increase in *Il4* and IL-13 expression by dopamine+IL-4 was greater than single treatment combined (Figures 2B, 2C and S1C). In addition, dopamine induced the appearance of IL-13$^+$ cells in Th0 cultures (6.14%) and increased the percentage of IL-13$^+$ cells in Th0+IL-4 cultures from 14.3% to 19.4% (Figure 2D). Furthermore, dopamine promoted T cell proliferation by ~20% in both Th0 and Th0+IL-4 cultures (Figure 2E). Because of the effect of dopamine on cell proliferation, the total number of IL-13$^+$ cells in dopamine-treated Th0+IL-4 culture was slightly higher than the combined effect of single treatment. Taken together, dopamine promotes Th2 cell differentiation in synergy with IL-4.

To evaluate whether age affected T cell responses to dopamine, we compared IL-13 expression in dopamine-treated CD4$^+$ T cells isolated from neonatal and adult mice. We found no difference in the extent of IL-13 induction by dopamine between neonatal and adult cultures (Figures 2F and 2G). In addition, dopamine similarly elevated *Il13* expression in human CD4$^+$ T cells isolated from lymph nodes associated with donor lungs from children and adults (Figure S1G). Furthermore, after identifying DRD4 as the functional dopamine receptor on CD4$^+$ T cells (Figure 3), we showed that age had no effect on DRD4

expression (Figure S2C). Therefore, dopamine promotes Th2 cell differentiation independently of age.

Dopamine promotes Th2 cell differentiation through a global transcriptional program.

To gain insights into the mechanism of dopamine signaling in Th2 cell differentiation, we performed RNA sequencing (RNA-seq) of day 4 Th0 cultures. Among a total of 1589 differentially expressed genes with an adjusted p-value<0.05 (Figure 2H), dopamine elevated the expression of Th2 cytokine genes, such as *Il4, Il5* and *Il13*, while repressing Th1 cytokine genes, such as *Ifng* and *Il12a* (Figure 2I). These findings were consistent with the results of qPCR and ELISA in culture (Figures 2A-2C, S1C and S1D). Dopamine also increased the expression of receptor genes for IL-2 and IL-4 (Figure 2I), suggesting a feed forward mechanism for these two essential cytokines in Th2 differentiation. Furthermore, dopamine upregulated the expression of the Th2-specifying gene, *Gata3*, as well as other transcriptional factors known to play a role in Th2 differentiation including *Maf* and *Pparg* (Chen et al., 2017; Henriksson et al., 2019; Ho et al., 1998; Zheng and Flavell, 1997) (Figure 2J). Genes involved in T cell activation during Th2 differentiation (Aki et al., 2018; Henriksson et al., 2019) were also changed by dopamine (Figure 2K). Notably, dopamine had no effect on the expression of *Il6, Il9, Il10* and *Il17* genes. Therefore, dopamine signaling selectively promotes Th2 cytokine expression in naïve CD4$^+$ T cells by activating a transcriptional program.

We generated a list of all genes detected in the samples ranked on the t-statistic followed by pathway analyses. We found dopamine regulated energy consumption, ion channel activity and cell cycle pathways (Figure 2L). These findings are consistent with the positive effect of dopamine on T cell proliferation (Figure 2E). We also found a significant overlap of differentially expressed genes between dopamine treatment and EZH2 deficiency in CD4$^+$ T cells (Figure 2L). EZH2 is a histone methyltransferase within the Polycomb Repressive Complex 2 (PRC2). EZH2 enzymatically catalyzes histone 3 trimethylation at lysine 27 (H3K27me3) to induce epigenetic silencing of gene expression (Margueron and Reinberg, 2011). These findings suggest that epigenetic mechanisms may be involved in dopamine-induced Th2 cell differentiation.

DRD4 is the functional dopamine receptor on CD4$^+$ T cells.

Among the 5 dopamine receptor genes (*Drd1-Drd5*), qPCR of naïve mouse CD4$^+$ T cells and RNA-seq of T cell cultures detected the mRNA expression of *Drd1, Drd4* and *Drd5* and that *Drd4* gene expression was the highest (Figure S2A). To confirm DRD4 expression by CD4$^+$ T cells, we stained the Th0 culture with a DRD4 antibody. The specificity of this DRD4 antibody was confirmed by negative staining of *Drd4$^{-/-}$* CD4$^+$ T cells (Figures 3A and 3E). DRD4 was detected on the surface of CD4$^+$ T cells in culture from mice and humans (Figure 3A) and its expression was unchanged by T cell differentiation, age and the location of CD4$^+$ T cells (in circulation or in tissue) (Figures S2B-S2D). A majority of CD4$^+$ T cells (97%) in human lymph nodes were DRD4$^+$ (Figure 3B).

DRD4 was not detected in the normal mouse lung by antibody staining likely due to a low abundance of CD4$^+$ T cells at baseline (Figure 3C). However, following allergen exposure to

neonatal mice, DRD4$^+$ cells appeared in close proximity to tyrosine hydroxylase$^+$ nerves around airways and blood vessels where immune cells were recruited into the lung (Figure 3D). To extensively characterize DRD4 expression in immune cells, we employed flow cytometry analyses. Because there is no commercially available flow antibody for DRD4, we used the DRD4 antibody for immunohistochemistry and included *Drd4$^{-/-}$* cells as negative control. CD4$^+$ T cells accounted for ~18% of all immune cell recruits following allergen exposure. DRD4 was expressed by a majority of the recruited CD4$^+$ T cells (76%) (Figure 3E). In contrast, other immune cells involved in type 2 inflammation, such as ILCs, B cells, mast cells, eosinophils and antigen-presenting cells (macrophages and dendritic cells), had no detectable DRD4 expression (Figures S2A and S2E). Given a significant role of ILCs in type 2 inflammation, we evaluated other four dopamine receptor genes and found no expression of any dopamine receptor genes in ILCs (Figure S2A). In accordance, dopamine had no effect on type 2 cytokine expression by ILCs or differentiated ILC2 cells in culture (Figures S2F-S2K). Lastly, ~20% of DRD4$^+$ cells were CD4$^-$ and these DRD4$^+$CD4$^-$ cells likely included CD8$^+$ T cells (Figure S2E).

DRD4 belongs to the D2 receptor subfamily that blocks adenylate cyclase, while DRD1 and DRD5 are D1 receptors that activate adenylate cyclase (Beaulieu and Gainetdinov, 2011). Dopamine reduced the amount of intracellular cyclic AMP (cAMP) from 35 fmol to 23 fmol per one million CD4$^+$ T cells (Figure 3F), further supporting DRD4 being the major dopamine receptor.

To test whether DRD4 was required for dopamine-induced Th2 differentiation, we first compared the effect of dopamine on *Il13* mRNA expression in cultures from wildtype and *Drd4$^{-/-}$* mice. Dopamine increased *Il13* gene expression in wildtype cells; however, it had no effect in *Drd4$^{-/-}$* cells (Figure 3G). Notably, we found no baseline difference in *Il13* mRNA between wildtype and *Drd4$^{-/-}$* cultures (Figure 3G). This finding is consistent with a lack of tyrosine hydroxylase expression by T cells (Figure 1J) and hence no baseline dopamine signaling. Secondly, a specific DRD4 antagonist L745870 (300 nM) (Patel et al., 1997) completely blocked the effect of dopamine on IL-13 expression in mouse and human CD4$^+$ T cells, while a DRD4-specific agonist, A412997 (100 nM) (Moreland et al., 2005) increased IL-13 expression (Figures 3H and 3I). Thirdly, SCH-23390 (50 nM, an inhibitor of DRD1/5) (Hyttel, 1983) and raclopride (50 nM, an inhibitor of DRD2/3) (Ogren et al., 1986) had no effect on dopamine-induced IL-13 expression (Figure 3J). These findings demonstrate that DRD4 is the functional receptor on CD4$^+$ T cells that mediates dopamine signaling in Th2 differentiation.

The dopamine-DRD4 pathway promotes Th2 cell differentiation by enhancing IL-2-STAT5 signaling.

Among the key regulators of Th2 cell differentiation, the expression of *Il2ra* is known to be repressed by cAMP (Anastassiou et al., 1992). Therefore, the dopamine-DRD4 pathway may increase the expression of IL-2Rα (also called CD25) by repressing cAMP production, thereby promoting IL-2 signaling and Th2 differentiation. In support of this hypothesis, dopamine elevated the *Il2ra* gene expression by RNA-seq (Figure 2I). Dopamine also

increased CD4^{+} T cell proliferation (Figure 2E), consistent with an enhanced, proliferative role of IL-2.

To test whether dopamine upregulated IL-2Rα expression and signaling by reducing cAMP production, we compared CD4^{+} T cell cultures treated with dopamine alone and in combination with forskolin (Fsk, 1 μM), an agonist of adenylate cyclase. Fsk completely prevented dopamine-induced increases in *Il2ra* gene expression and the percentage of CD25^{+}CD4^{+} T cells in both Th0 and Th0+IL-4 cultures (Figures 4A, 4B, S3A and S3E). Consistent with increased IL-2Rα expression, dopamine significantly elevated the signaling activity of IL-2, as shown by increased STAT5 phosphorylation (p-STAT5) in Th0+IL-4 cultures (Figures 4B and S3I). However, the amount of p-STAT5 was reduced almost to baseline by Fsk (Figures 4B and S3I). We then tested whether elevated IL-2 signaling by dopamine was required for the increase in Th2 cytokine expression. For this assay, we treated Th0 cultures with a specific STAT5 inhibitor, CAS285986-31-4 (Muller et al., 2008). To diminish the side effect of the inhibitor on cell survival, we tested different concentrations of the inhibitor and the duration of treatment. The STAT5 inhibitor at 20 μM had no detectable effect on cell growth and baseline expression of CD25 and IL-13 in day 2 cultures (Figures 4C, 4D, S3J and S3K); however, the STAT5 inhibitor abolished the induction of CD25 and IL-13 expression by dopamine (Figures 4C, 4D, S3J and S3K). Lastly, to link cAMP production and Th2 cytokine gene regulation in the dopamine-DRD4 pathway, we analyzed IL-13 and *Il4* expression in Th0 and Th0+IL-4 cultures that were treated with dopamine alone or dopamine+Fsk. The combined treatment diminished the increase in IL-13 and *Il4* expression in dopamine-treated cultures (Figures S3B-S3D and S3F-S3H). Therefore, the dopamine-DRD4 pathway blocks cAMP production to upregulate IL-2Rα expression thereby elevating IL-2 signaling activities to promote Th2 differentiation.

Dopamine transcriptionally upregulates Th2 genes with associated reduction in H3K27me3 at these Th2 gene loci.

Pathway analysis of RNA-seq data suggested that dopamine signaling in CD4^{+} T cells may involve epigenetic mechanisms by counteracting the activity of EZH2 (Figure 2L). EZH2 is known to bind directly to the promoter of Th2 genes, such as *Gata3, Il4, Il5* and *Il13*, and repress gene transcription by causing H3K27me3 (Tumes et al., 2013). To test whether dopamine reduced H3K27me3 at the Th2 gene loci, we performed ChIP with a specific H3K27me3 antibody followed by qPCR using primers flanking the established EZH2-binding sites within the promoter of the Th2 genes (Tumes et al., 2013). Compared to untreated control, dopamine reduced H3K27me3 at the promoters of *Il4, Il5* and *Il13* genes in Th0 and Th0+IL-4 cultures (Figures 4E and 4F). For the *Gata3* promoter, dopamine decreased H3K27me3 at the −5kb and −4kb sites but not at the +3kb site (Figures 4E and 4F). In contrast, dopamine had no effect on H3K27me3 in the promoter of *Il2ra*, a gene that exhibited little EZH2 binding (Tumes et al., 2013) (Figures 4E and 4F). Taken together, dopamine signaling decreases epigenetic silencing of selected Th2 genes, which may facilitate Th2 cell differentiation.

To test if dopamine opposed EZH2 to mediate epigenetic modification, we showed that dopamine reduced the expression of *Ezh2* and 3 regulatory subunit genes within PRC2, *Eed,*

Jarid2 and *Aebp2* (Figure S3L). In addition, blockade of the EZH2 activity by a specific inhibitor, 3-deazaneplanocin A (DZNep), similarly promoted Th2 cytokine expression as dopamine (Figures S3M and S3N) (Tumes et al., 2013). Importantly, DZNep blunted the effect of dopamine on *Il4* and *Il13* gene expression in culture (Figures S3M and S3N). As a control for the functional specificity of DZNep, we showed DZNep had no effect on *Il2ra* gene with and without dopamine (Figure S3O). These findings support that dopamine-induced Th2 differentiation involves epigenetic regulation at key Th2 gene loci by repressing EZH2 and other components within PRC2.

The dopamine-DRD4 pathway plays a critical, augmenting role in Th2 inflammation following allergen exposure in neonatal mice, but not in adult mice.

The dopaminergic-to-adrenergic transition of the sympathetic nervous system during postnatal development was associated with more dopamine in the early lung than the adult lung (Figure 1). We reasoned that if dopamine served as an age-related neural signal to augment Th2 cell differentiation, blockade of the dopamine-DRD4 signaling would preferentially ameliorate Th2 inflammation in early life. To test this hypothesis, we assessed the effect of DRD4 inhibition on Th2 inflammation in neonatal and adult mice following the exposure to house dust mite (HDM) or ovalbumin (OVA) (Figures 5 and S4-S6). To block DRD4, we employed the specific DRD4 inhibitor (L745870) and *Drd4^{−/−}* mice. Notably, *Drd4^{−/−}* mice have no previously reported phenotypes except for addictive behavior (Rubinstein et al., 1997). Consistently, no baseline lung phenotype was found in L745870-treated mice and *Drd4^{−/−}* mice without allergen exposure (PBS condition) (Figures 5E, 5M, S5C-S5I and S5S).

Neonatal mice were sensitized and challenged intranasally with HDM and treated with L745870 between P10-P20 (Figure 5A), a time period when tyrosine hydroxylase expression increased sharply in the lung (Figure 1A). Due to technical issues of neonatal intranasal delivery that often causes variation in the efficacy, we chose to deliver L745870 by intraperitoneal injection. At P21, compared to solvent, L745870 reduced the amount of IL-5 and IL-13 (Figure 5B) and diminished the abundance of lymphocytes and eosinophils in BALF (Figure 5C). L745870 also significantly decreased the number of IL-5- and IL-13-expressing CD4$^+$ T cells and eosinophils in the lung (Figures 5D and S4A). In addition, L745870 decreased HDM-induced mucus overproduction and the amount of total IgE in serum and ameliorated airway hyperresponsiveness to methacholine (Figures 5E-5H). Furthermore, L745870 improved pathological scores in the HDM-exposed lung as assayed by the thickness of airway epithelium and peri-vascular nuclear density (Figures S4B and S4C). Lastly, similar to L745870 treatment, genetic disruption of DRD4 reduced Th2 inflammation in neonatal mice following HDM exposure (Figures S4D-S4F).

We assessed the effect of L745870 in the adult HDM mouse model (Figure 5I). The dosage of HDM was adjusted to the body weight of adult mice. Adult mice that were treated with L745870 for the same duration as neonates exhibited no significant difference in Th2 inflammation compared to solvent treatment (Figures 5J-5O and S4G-S4I).

As a complementary model of allergic inflammation, we subjected neonatal and adult mice to OVA sensitization and challenge (Figures S5 and S6). We showed that L745870 treatment

and DRD4 deficiency profoundly reduced Th2 inflammation, airway hypercontractility and mucus overproduction following OVA exposure in neonates, while having a marginal effect in adult mice (Figures S5 and S6). Taken together, the dopamine-DRD4 pathway plays an age-related role in augmenting Th2 inflammation in early life.

Allergen exposure had no effect on the age-related reduction in the expression of tyrosine hydroxylase (Figure S5B) and neonatal DBH expression (Figure S5M). In accordance, the amount of dopamine remained unchanged in allergen-exposed mouse lung at P21 (898.2±95.57 pg/mg lung weight (OVA) versus 961.9 ± 66.72 pg/mg lung weight (PBS)). However, DBH expression in the adult lung was elevated by allergen exposure (Figure S5M). This was associated with a decrease in the already lower amount of dopamine (229.4±73.08 pg/mg lung weight (OVA) versus 494.0 ± 114.7 pg/mg lung weight (PBS)). Therefore, allergen exposure potentiates the age-related difference in dopamine.

Dopamine in the lung is a critical, age-related regulator of Th2 inflammation.

To provide further evidence that the age-related role of dopamine-DRD4 signaling in allergic inflammation was determined by the amount of dopamine, we assessed the impact of dopaminergic neuron ablation on Th2 inflammation in neonates following allergen exposure. For this assay, mice were treated with 6OHDA, a specific neurotoxin for dopaminergic neurons during the first 2 weeks after birth (Angeletti and Levi-Montalcini, 1972) (Figure 6A). 6OHDA diminished tyrosine hydroxylase+ nerves in the lung at P21 (Figures 6F and 6G). 6OHDA treatment had no detectable effect on inflammation at baseline (Figures 6B-6L). However, following OVA exposure, mice treated with 6OHDA exhibited a significant reduction in IL-5 and IL-13 (Figure 6B) and the abundance of lymphocytes and eosinophils in the BALF (Figure 6C). 6OHDA also reduced the abundance of IL-13+CD4+ T cells and eosinophils in the lung (Figures 6D and 6E), the amount of p-STAT6 (Figures 6F and 6H), mucus overproduction (Figures 6I and 6J) and the amount of total IgE in serum (Figures 6M). Furthermore, 6OHDA improved pathological scores in OVA-exposed lungs measured by airway epithelial thickness and perivascular nuclear density (Figures 6K and 6L).

6OHDA has a broad impact on the sympathetic nervous system. To alleviate the concern of side effect of 6OHDA, we took a complementary, gain-of-function approach by treating adult mice with a specific DRD4 agonist, A412997 (Moreland et al., 2005), to offset the low dopamine activity in the adult lung (Figure S7A). DRD4 activation alone was insufficient to induce inflammation (Figure S7B). Following OVA exposure, the DRD4 agonist substantially worsened Th2 inflammation and mucus overproduction in adult mice (Figures S7C-S7G). Taken together, the amount of dopamine is a critical regulator of Th2 inflammation in the lung.

CD4+ T cells mediate dopamine-DRD4 signaling in early life to augment Th2 inflammation.

To establish that CD4+ T cells were the critical mediator of dopamine-DRD4 signaling in the early lung, we performed adoptive transfer assay using CD4+ T cells isolated from OT-II mice. OT-II mice express a transgenic T cell receptor for OVA. OVA sensitization of OT-II mice stimulated T cell activation and proliferation (Church et al., 2012; Kim et al., 2018),

evident by a 3-fold increase in the number of splenic $CD4^+$ T cells with a significant, activated $CD44^{high}CD62L^{low}$ subpopulation (~25%). Since age had no effect on T cell response to dopamine (Figures 2F, 2G and S1G), we isolated $CD4^+$ T cells from 5-week-old OTII mice for the adoptive transfer assay because the spleen at this age is fully grown and contains more $CD4^+$ T cells than the neonatal spleen. Purified splenic $CD4^+$ T cells from OVA-sensitized OT-II mice were intra-tracheally transferred into wildtype and $Drd4^{-/-}$ recipients at P14 followed by OVA challenge (Figure 7A). Since the recipients were not sensitized, OVA challenge induced allergic inflammation only through the transferred OT-II cells. At P21, wildtype and $Drd4^{-/-}$ recipients exhibited comparable Th2 inflammation, as assayed by the amount of IL-5 and IL-13 and the number of eosinophils in BALF (Figures 7B and 7C), infiltrating $IL-13^+CD4^+$ T cells and eosinophils in the lung (Figures 7D and 7E), the amount of p-STAT6 (Figures 7F and 7G), mucus overproduction (Figures 7H and 7I) and pathological scores (Figure 7J). These findings indicate that the adoptively transferred $CD4^+$ T cells from OVA-sensitized OT-II mice are sufficient to induce allergic inflammation in neonates independent of the genotype of the recipient.

After validating the adoptive transfer approach in neonatal allergic inflammation, we went on to evaluate the contribution from the transferred OT-II cells and the recipient to dopamine-augmented allergic inflammation. For this assay, we treated wildtype and $Drd4^{-/-}$ recipient mice with the DRD4 inhibitor, L745870 immediately after the adoptive transfer at P14 (Figure 7A). We reasoned if cells from recipient mice played a role in DRD4 regulation of allergic inflammation, L745870 treatment would have a greater inhibitory effect on wildtype littermates than $Drd4^{-/-}$ mice. However, we found that L745870 treatment similarly reduced Th2 inflammation regardless of the recipient genotype as shown by immunological assays of Th2 inflammation, mucus overproduction and pathological scores (Figures 7B-7J). Therefore, the transferred $CD4^+$ T cells from OVA-sensitized OT-II mice primarily mediate dopamine-DRD4 signaling in the early lung to augment Th2 inflammation. These findings, together with selective expression of DRD4 in $CD4^+$ T cells, but not ILCs and other immune cells involved in type 2 inflammation (Figures 3A, 3B, S2A and S2E), provide strong evidence that $CD4^+$ T cells are the critical mediator of dopamine signaling in the early lung to promote Th2 inflammation.

Discussion

In this study, we have discovered that the development of sympathetic innervation provides a critical mechanism underlying the susceptibility to allergic asthma in early life. We show that sympathetic nerves are dopaminergic during the postnatal development of the lung. By releasing dopamine that induces Th2 cell differentiation, the immature sympathetic nervous system equips the early lung with a dopamine-enriched environment that fosters allergic inflammation. With age, sympathetic nerves mature into an adrenergic phenotype. Norepinephrine and epinephrine released from the adrenergic nerves have no effect on Th2 cell differentiation activity likely due to low adrenergic receptor expression as shown by RNA-seq. Therefore, the dopaminergic-to-adrenergic transition of sympathetic innervation plays an age-related role in allergic inflammation. Our study identifies DRD4 as the functional receptor for dopamine in Th2 cell differentiation. DRD4 is selectively expressed by T cells, but not ILCs. The differential expression of DRD4 in T cells and ILCs, together

with previous findings that epinephrine negatively regulates ILC2 (Moriyama et al., 2018), highlights the complexity and specificity of neural regulation of type 2 inflammation.

We provide evidence that humans and mice exhibit a similar, dopaminergic-to-adrenergic transition of sympathetic nerves during postnatal development of the airway. The conservation of this transition during evolution suggests that dopaminergic innervation may provide some advantage when the lung is immature and vulnerable to infection. One possibility is that by facilitating type 2 inflammation, dopaminergic nerves endow the early lung with a mechanism of tissue repair following infection and eradication of parasitic worms. It is also possible that in the context of the physiological role of norepinephrine in vasoconstriction of pulmonary vessels (Tuck, 1986), the dopaminergic phenotype in the early lung may support vascular development by preventing premature vascular constriction.

We show the major source of dopamine is the nerves that innervate the airway and vasculature in the lung and lymphatic vessels in associated lymph nodes. While the amount of dopamine released from the activated nerve is difficult to measure, the local concentration of dopamine can reach up to the range of hundreds of μM to mM upon firing of the nerve (Goto et al., 2007). Therefore, we speculate that the active, micromolar range of dopamine in Th2 cell differentiation may be physiologically relevant. In addition to a direct communication between nerves and T cells, we can't exclude the possibility that dopamine released by nerves may be transported through specific dopamine transporters or non-specifically taken up by immune cells, such as dendritic cells and macrophages. This possibility is supported by previous reports that dopamine can be detected in some immune cells by HPLC without the evidence of tyrosine hydroxylase expression (Bergquist and Silberring, 1998; Cosentino et al., 2007; Josefsson et al., 1996; Nakano et al., 2009). In this scenario, dendritic cells may transport dopamine to T cells in the lymph node where dendritic cells present allergen to initiate T cell differentiation, thereby serving as an indirect means of neural regulation of Th2 cell differentiation through the dopamine-DRD4 pathway.

The expression and function of DRD4 in CD4$^+$ T cells is supported by previous studies in human samples (Kustrimovic et al., 2014; Sarkar et al., 2006). However, there are conflicting reports of dopamine receptor expression and signaling in T cells and mouse models. The conflict may be explained by the caveat of detection using non-quantitative PCR assays of CD4$^+$ T cells (Contreras et al., 2016; Franz et al., 2015; Huang et al., 2010; Ilani et al., 2004). In addition, the inflammation defects in *Drd3–/–* mice may be unspecific to T cells (Contreras et al., 2016), as the cell type specificity of DRD3 expression is not well-characterized. Furthermore, small molecule dopamine receptor inhibitors may have off-target effects, which complicates the functional study of a specific dopamine receptor in inflammation. For example, a D1 receptor antagonist, SCH-23390 may also interfere with DRD4 (*Ki*=1.1 μM) (Bourne, 2001) at a concentration of 1 μM used in previous studies (Mori et al., 2013; Nakano et al., 2009).

Our results show that the dopamine-DRD4 pathway plays an augmenting role in Th2 cell differentiation by interacting with IL-2 and IL-4. We have provided evidence that the functional interaction between dopamine and IL-2 is mediated at least in part by the cAMP pathway. Considering a variety of signals in allergic inflammation that are known to

upregulate cAMP production through commonly expressed receptors, the dopamine-DRD4 pathway uniquely represses cAMP production thereby upregulating IL-2Rα expression. In addition, dopamine signaling is associated with reduced H3K27me3 in Th2 gene loci, an epigenetic mechanism that may facilitate Th2 gene transcription in synergy with IL-4. Based on the RNA-seq data, we speculate that the epigenetic mechanism may be mediated by the reduction in the expression of *Ezh2, Eed, Jarid2* and *Aebp2*, the components of PRC2 that causes H3K27me3 to suppress gene transcription (Margueron and Reinberg, 2011). RNA-seq also showed that dopamine upregulated the expression of several transcriptional factors required for IL-4-induced Th2 cell differentiation, such as *c-Maf, Irf4, Xbp1* and *Bhlhe40* (Henriksson et al., 2019), which may provide another mechanism underlying the synergic interaction between dopamine and IL-4. Whether changes in the expression of candidate epigenetic regulators and the transcriptional factors are regulated by the cAMP pathway warrants further investigation.

Previous clinical and basic studies showed that the immature immune system is poised towards type 2 inflammation (de Kleer et al., 2016; Hebel et al., 2014). Our study suggests that dopaminergic nerves in the early lung may potentiate an already type 2-poised immune system thereby contributing to the susceptibility to allergic asthma in early childhood (Stern et al., 2008). Importantly, our findings reveal the similarity of dopaminergic innervation of the early lung and the T cell response to dopamine between mice and humans. The identification of dopamine-specific gene signature in Th2 cells will facilitate future study of dopamine regulation of allergic asthma in children. Based on RNA-seq data, several dopamine-regulated genes in mouse CD4$^+$ T cells have established disease relevance. For example, among the downregulated genes by dopamine, cAMP-responsive element modulator (CREM) has also been shown to exhibit a reduced expression in CD4$^+$ T cells from children with recurrent and persistent wheeze compared to healthy controls (Verjans et al., 2015). In addition, dopamine upregulates *Il2ra, Il7r* and *Crlf2 (Tlspr)*, all of which were identified to be associated with the susceptibility to allergic asthma (Ferreira et al., 2017; Sherrill et al., 2010).

To understand the mechanism underlying the dopaminergic-to-adrenergic transition of sympathetic nerves in the developing lung, future studies are required to map the subset of sympathetic neurons that specifically supply the lung and to identify neurogenic signals required for the development of these neurons. Neurons dynamically interact with target tissues during development. It is possible that the innervating sympathetic neurons may decrease the expression of tyrosine hydroxylase, while upregulating DBH to fully differentiate into the adrenergic phenotype during postnatal maturation. Members of the neurotrophin family, such as nerve growth factor and brain-derived neurotrophic factor have established roles in the development of sympathetic neurons (Barbacid, 1994). We have shown that lung innervation requires neurotrophins (Aven et al., 2014; Patel et al., 2016; Radzikinas et al., 2011). Therefore, neurotrophins may regulate sympathetic innervation of the lung. Clinical studies have shown that the amount of nerve growth factor and brain-derived neurotrophic factor is aberrantly regulated in infants following infection with respiratory syncytial virus (Tortorolo et al., 2005). In addition, brain derived neurotrophic factor expression has been shown to be positively associated with the severity of allergic asthma (Watanabe et al., 2015). The identification of the neurotrophic factors that regulate

the dopaminergic-to-adrenergic transition of sympathetic innervation may provide insights into the connection between respiratory viral infection in early life and allergic asthma.

In summary, our findings indicate that developing, dopaminergic nerves in the airway contribute to the susceptibility to allergic inflammation in the early life. Targeting the communication between sympathetic nerves and CD4$^+$ T cells via the dopamine-DRD4 pathway may be a strategy to battle the increasing prevalence of allergic asthma in children.

STAR METHOD

LEAD CONTACT AND MATERIALS AVAILABILITY

Further information and requests for resources and reagents should be directed to and will be fulfilled by the Lead Contact, Xingbin Ai (xai@partners.org). This study did not generate new unique reagents.

EXPERIMENTAL MODELS AND SUBJECT DETAILS

Mice.—C57BL/6 (B6), *Drd4*$^{+/-}$ mice (stock number: 008084) and OT-II mice (stock number: 004194) were purchased from The Jackson Laboratories and were maintained in the SPF animal facility at Brigham and Women's Hospital, Harvard Medical School. All animal experiments were approved by the Institutional Animal Care and Use Committee. *Drd4*$^{+/-}$ mice were bred to produce *Drd4*$^{-/-}$ mice and control, wildtype littermates. Both male and female mice were used for experiments. Unless specified for the age of mice, adult mice at 3-4 months of age were used.

Human donor lungs.—Lungs from de-identified, male and female donors between 0-65 years of age were purchased from International Institute for the Advancement of Medicine (IIAM), a non-profit institute that provides non-transplantable human tissues for medical research. 4 adult lungs (1 female and 3 male donors of 40-65 years of age) and 4 lungs from children (1 female, 2 males and 1 unknown, 0-13 years of age) were used in this study. These donors were healthy volunteers, had no previous lung diseases, and mostly died of brain injuries and heart failure. All the information regarding the donor is anonymous. Because the experiment involves no intervention or interaction with the donors and relates to no living individuals, this project is deemed non-human subject research by the IRB committee at Brigham & Women's Hospital.

METHOD DETAILS

Neonatal and adult mouse models of allergic inflammation.—For the neonatal model of OVA exposure (Aven et al., 2014), pups were sensitized by intraperitoneal injection of 10 μg OVA (Sigma Aldrich, A5503) in Imject alum (Thermo Scientific, 77161) at postnatal day 5 (P5) and P10. Mice were subjected to aerosolized challenges of 3% OVA solution between P18-P20, 20 minutes per day. For the neonatal model of HDM exposure (Barrios et al., 2017), pups were sensitized intra-nasally with 2 μg HDM (Greer Laboratories, XPB70D3A25) in PBS at P5 and P10. Mice were then intra-nasally challenged on 5 consecutive days between P16- P20, each day with 10 μg HDM. For both neonatal models of allergen exposure, mice were euthanized at P21. For the adult model of OVA

exposure, adult mice were sensitized with 50 μg OVA in Imject alum on experimental day 0 (D0) and Day 5 followed by 3 aerosolized OVA challenges between D13-D15. For the adult model of HDM exposure, mice were sensitized intra-nasally with 10 μg HDM in PBS at D0 and D5. Mice were then intra-nasally challenged on 5 consecutive days between D11-D15, each day with 25 μg HDM. For both adult models of allergen exposure, mice were euthanized at D16. Non-allergic control mice of both age groups were challenged with saline. For the treatment with the DRD4 antagonist L745870 (Sigma Aldrich, L131), mice were injected intra-peritoneally L745870 at 1 mg/kg body weight (Patel et al., 1997) on a daily basis between P10-P20 for the neonatal model and experimental day 5-day 15 for the adult mouse model. For ablation of dopaminergic nerves, mice were injected subcutaneously 6OHDA (Tocris, 2547) at 100 mg/kg body weight once a day between P1-P7 and got another injection on P14 (Angeletti and Levi-Montalcini, 1972). For the treatment with the DRD4 agonist A412994, adult mice were injected intra-peritoneally with A412994 (Sigma Aldrich, SML0608) once per day between experimental day 12-day 15. A412994 was given at 0.1 μmol/kg body weight (Moreland et al., 2005). For adoptive transfer, donor OT-II mice at 5 weeks of age were sensitized twice and total $CD4^+$ T cells were purified from spleen using an isolation kit (Miltenyi Biotec, 130-104-454). 2×10^6 $CD4^+$ T cells were adoptively transferred to each WT or $Drd4^{-/-}$ mouse when the recipients were P14. The recipients were then injected intra-peritoneally L745870 at 1 mg/kg body weight once a day between P14-P20 and challenged with OVA daily between P18-P20. Bronchoalveolar lavage fluid (BALF), lungs and blood samples were collected 24 hours after the last challenge in both neonatal and adult models (Aven et al., 2014).

Mouse primary lymphocyte preparation and culture.—Mice were sacrificed by over-inhalation of isoflurane followed by cervical dislocation. Spleens were isolated, minced and digested in RPMI-1640 (Life Technologies, 11875-119) with 10% FBS, 400 U/mL Collagenase Type 4 (Worthington-Biochem, LS004188), 0.1% Dispase II (Sigma, 4942078001) and 20 μg/mL DNase I (NEB, 439807) for 30 min at 37°C. For each sample, 12 mL of digestive solution was used. Digested spleens were mechanically disrupted by pushing through syringe with 18-gauze needle and passage through 100 μm and 40 μm wire meshes. Cells were pelleted by centrifugation and re-suspended in 2 mL red blood cell lysis buffer (Sigma Aldrich, R7757) to remove red blood cells. Naïve $CD4^+$ T cells were enriched by negative selection using an isolation kit (Miltenyi Biotec, 130-104-453). $CD4^+CD25^-CD44^-CD62L^+$ cells were deemed naïve $CD4^+$ T cells that accounted for ~95% of the purified cell population. Purified cells (2×10^6 per well) were cultured in a 12-well plate pre-coated with 1 μg/mL αCD3 (BD Biosciences, 553058). RPMI-1640 medium was supplemented with 10% FBS, 100 U/mL penicillin, 0.1 mg/mL streptomycin, 2 mM 2-mercaptoethanol. For Th0 condition, cells were cultured at the presence of 1 μg/mL αCD28 (BD Biosciences, 553295). For Th2 (Th0+IL-4) condition, cells were cultured at the presence of 1 μg/mL αCD28, 5 ng/mL rmIL-2 (R&D Systems, 402-ML-010) and 10 ng/mL rmIL-4 (BioLegend, 574302). For Th1 condition, cells were cultured at the presence of 1 μg/mL αCD28, 5 ng/mL rmIL-2 (R&D Systems, 402-ML-010) and 10 ng/mL rmIL-12 (R&D Systems, 419-ML-010). For Th17 condition, cells were cultured at the presence of 1 μg/mL αCD28, 5 ng/mL rmIL-2 (R&D Systems, 402-ML-010), 2 ng/mL rhTGF-β (R&D Systems, 240-B-002) and 20 ng/mL rmIL-6 (R&D Systems, 406-ML-005) for 48h. And then

10 ng/mL rmIL-23 (R&D Systems, 1887-ML-010) was added to the culture. For treatment, individual neurotransmitter was added daily to T cell cultures on day 0 to day 2. These included dopamine (0.1- 25 μM, Fisher Scientific, 35-485-0), epinephrine (10 μM, Sigma Aldrich, E4250) and norepinephrine (10 μM, Sigma Aldrich, A7257). For most of cultures with dopamine, 10 μM dopamine was used. Other pharmaceutical reagents used in culture to modulate the dopamine pathway include: L-745,870 hydrochloride (300 nM, Sigma Aldrich, L131), raclopride (50 nM, Sigma Aldrich, R121), SCH-23390 hydrochloride (50 nM, Sigma Aldrich, D054), A-412997 dihydrochloride (100 nM, Sigma Aldrich, SML0608), forskolin (1 μM, Tocris, 1099), CAS285986-31-4 (20 μM, Sigma Aldrich, 573108), DZNep (7.5 nM, EMD Millipore, 252790-2MG). For treatment with CAS285986-31-4, cultures were analyzed on day 2. For all other cultures, cells and the conditioned media were harvested for gene and cytokine expression assays after 4 days in culture.

Primary human lymphocyte isolation and culture.—Mediastinal lymph nodes associated with healthy donor lungs were dissected digested with 400 U/mL Collagenase Type 4, 0.1% Dispase II and 20 μg/mL DNase I for 30 min at 37°C. Digested samples were mechanically disrupted by pushing through syringe with 18-gauze needle and passage through 100 μm and 40 μm wire meshes. Naïve CD4$^+$ T cells were enriched by negative selection using isolation kits (Miltenyi Biotec, 130-094-131). Purified cells (2×10^6 per well) were cultured in a 12-well plate pre-coated with 2 μg/mL αCD3 (eBioscience, 16-0037-85). RPMI-1640 medium was supplemented with 10% FBS, 100 U/mL penicillin, 0.1 mg/mL streptomycin, 2 mM 2-mercaptoethanol. For Th0 condition, cells were cultured at the presence of 2 μg/mL αCD28 (BD Biosciences, 555725). For Th2 (Th0+IL-4) condition, cells were cultured at the presence of 2 μg/mL αCD28, 5 ng/mL rhIL-2 (R&D Systems, 202-IL-010) and 10 ng/mL rhIL-4 (BioLegend, 204-IL-010).

Histology and antibody staining.—Lungs and mediastinal lymph nodes associated with donor lungs were fixed in 4% paraformaldehyde in PBS overnight. After washing, tissues were processed for paraffin embedding and cryopreservation before paraffin sections (5 μm) and frozen sections (15 μm), respectively, were collected. Frozen sections were used for visualizing nerve fibers in Figure 1. For staining of cells in culture, cells were spun onto histological slides using a cytospin centrifuge before fixation. The procedure of antibody staining was previously described (Aven et al., 2014). Primary antibodies included: mouse anti-DRD4 (1:100; EMD Millipore, MABN125), rabbit anti-tyrosine hydroxylase (1:200; EMD Millipore, AB152), rabbit anti-DBH (1:100; EMD Millipore, AB1585), mouse anti-neural class III b-tubulin (TUBB3) antibody (1:200; R&D Systems, MAB1195) and rabbit anti-CD4 (1:400; Novus Biologicals, NBP1-19371SS). For staining of mouse tissue sections using mouse monoclonal primary antibodies, tissue sections were blocked using the Mouse on Mouse Kit (Vector Laboratories, BMK-2202). Biotinylated secondary antibodies and secondary antibodies conjugated with Alexa Fluor®488 and 546 were purchased from Thermo Fisher Scientific. For fluorescence staining, nuclei were stained with Hoechst dye (1:1000) and images were collected by confocal microscopy (Carl Zeiss, LSM 710). For DAB staining, sections were treated with standard ABC kit (Vector Labs, PK-6100) and DAB Peroxidase Substrate Kit (Vector Labs, SK-4100). After DAB staining, samples were counterstained with Hematoxylin QS (Vector Laboratories, H-3404). Mucus in lung sections

was stained using periodic acid–Schiff (PAS) staining kit (Sigma-Aldrich, 395B-1KT). Bright field images were taken using a digital camera (Nikon DS-Fi2). To quantify sympathetic innervation, the immunoreactive areas of tyrosine hydroxylase and TUBB3 was quantified from non-overlapping images using Image J (National Institutes of Health, Bethesda, MD, USA) followed by the calculation of the ratio between tyrosine hydroxylase and TUBB3. To quantify pathological features of the lung (Cohen et al., 2007), 3 non-overlapping areas were quantified from one section, 3 sections for each mouse. The thickness of the airway epithelium was measured using Image J. The peri-vascular nuclear density was measured by quantifying the number of infiltrating cells in the peri-vascular area based on nuclear staining and then normalizing the number of nuclei to the size of the area measured by Image J.

Flow cytometry analysis of T cell cultures, BALF and lung samples.—Mouse lungs were enzymatically dissociated into single cell preparation, as described in the preparation of mouse lymphocytes from the spleen. For cell surface marker staining, cells were first stained with eBioscience™ Fixable Viability Dye eFluor™ 520 or 780 (1:2000) in PBS at 4°C for 30 min. After washing twice, cells were subjected to cell surface markers staining in FACS buffer (5% BSA and 0.1% sodium azide in PBS) at 4°C for 30 min. For intracellular cytokine staining, cells were treated with eBioscience™ Cell Stimulation Cocktail (plus protein transport inhibitors) (eBioscience, 00-4975-03) for 4 hr before live/ dead cell staining. Cells were then treated with fixation/permeabilization solution (BD Biosciences, 554722) before staining. For nuclear staining, cells were fixed in 4% paraformaldehyde for 30 min, permeabilized in 90% methanol at 4°C for 45 min and then stained with the antibody in FACS buffer at 4°C for 30 min. After staining, cells were first gated on CD45 and viability dye for live leukocytes. Doublets were excluded based on FSC-A vs. FSC-H and SSC-W vs. SSC-H. Among $CD3^+CD4^+$ T cells, the $CD62L^+CD44^-CD25^-$ population were deemed naïve $CD4^+$ T cells. Eosinophils were the Siglec F^+CD11c^{low} population. Macrophages were $CD11c^+$Siglec F^+MHC II^{low}. Dendritic cells were CD11c $^+$Siglec F^+MHC II^{high}. Neutrophils were $CD11b^+Ly6G^+$Siglec F^-MHC II^-. Mast cells were FceRlα $^+$c-Kit$^+CD11b^-CD11c^-$. Lymphocytes include T cells ($CD3^+CD19^-$), B cells ($CD19^+CD3^-$) and NK cells ($NK1.1^+CD3^-$). For flow cytometry analyses of DRD4 expression, cells were treated with the Mouse on Mouse Kit before incubated with the mouse anti-DRD4 antibody (1:100; EMD Millipore, MABN125) and a fluorescent secondary antibody. Cells were then double labelled for surface markers of $CD4^+$ T cells, $CD8^+$ T cells, B cells, eosinophils, mast cells, macrophages and dendritic cells. After staining, cells were analyzed on BD FACSCANTO II. Flowjo v.10.5.3 was used for data analysis. All the antibodies used for flow cytometry were listed in Key Resource Table.

ILCs isolation and culture.—Cells from the dissociated adult mouse lungs were incubated with CD90.2 microbeads (Miltenyi Biotec, 130-049-101) for 17 min on ice and enriched for $CD90.2^+$ cells by positive selection using LS columns (Miltenyi Biotec, 130-042-401). $CD90.2^+$ cells were stained with antibodies for 20 min on ice, washed and resuspended in complete medium. ILCs were defined as $CD45^+$ $CD90.2^+CD127^+ST2^+$ and negative for CD3, CD4, CD8, CD11b, CD11c, CD19, NK1.1, TCRβ, TCRγδ. ILCs were isolated by fluorescence activated cell sorting using a BD FACS Aria III. Cells were plated

at a density of 6,000 cells per well in complete medium and cultured with IL-7, IL-7 + dopamine, IL-7 + IL-33 or IL-7 + IL-33 + dopamine. IL-7 was used at a final concentration of 20 ng/ml, IL-33 at 200 ng/ml and dopamine at 10 μM. After 3 days in culture, ILCs were subjected to gene expression analyses and the supernatant was analyzed by ELISA.

Physiological measurements of airway reactivity.—For airway resistance assay, mice were injected with xylazine (10 mg/kg body weight), pentobarbital (100 mg/kg body weight) and pancuronium (0.5 mg/kg body weight), intubated and placed on a mechanical ventilator (Legacy flexiVent, SCIREQ). Ventilation was at 300 breaths/min (tidal volume 6–7 mL/kg body weight). Airway resistance was measured after airway delivery of nebulized methacholine in PBS (5 mg/mL, 15 mg/mL and 25 mg/mL). Data are presented as relative peak resistance to baseline within each experimental group. For airway contractility assay using lung slices, mouse lungs were infused with 1.5% low-melting agarose and sliced at 150 μm thickness using a tissue slicer (Precisionary Instruments Inc.). After overnight recovery in DMEM/F-12 (1:1; Life Technologies, 11320-033), lung slices were stimulated with increasing doses of methacholine (Sigma-Aldrich, A2251). Mid-sized airways with the diameter between 200-500 μm were imaged before stimulation and 5 min after stimulation with an inverted microscope (DMI6000B; Leica Microsystems, Buffalo Grove, IL, USA). The luminal area of the imaged airway was measured with Image J (National Institutes of Health, Bethesda, MD, USA). Airway contraction in response to methacholine was calculated as the percentage of reduction in the luminal area from the baseline.

Cell proliferation assay.—Cell proliferation was analyzed with CFSE Cell Division Tracker Kit (BioLegend, 423801) following the manufacturer's protocol. Briefly, freshly isolated lymphocytes were incubated with 5 μM CFSE in PBS containing 5% FBS for 20 min at room temperature and protected from light. The staining was quenched by washing twice with RPMI-1640 with 10% FBS. The labeled lymphocytes were then cultured before flow cytometry analysis.

Quantitative Real Time PCR (qPCR).—Total RNA was extracted from cultured T cells and lungs using a RNeasy kit (Qiagen, 74106) followed by reverse transcription using Superscript III Reverse Transcriptase (Thermo Fisher Scientific, 18080-044). For ILCs in culture, total RNA was extracted using PicoPure RNA isolation kit (Thermo Fisher Scientific, KIT0204) and reverse transcribed using SuperScript IV VILO Master Mix (Thermo Fisher Scientific, 11756050). Real time PCR was performed using CFX96 real-time system (Bio-Rad). TaqMan primers for mouse *Il13* (Mm00434204_m1), mouse *Il4* (Mm00445259_m1), mouse *Il5* (Mm00439646_m1), mouse *Areg* (Mm00437583_m1), mouse *Il2ra* (Mm01340213_m1), mouse *Muc5ac* (Mm01276704_m1), mouse *Ifng* (Mm01168134_m1), mouse *18S* rRNA (Mm03928990_g1), human *Il13* (Hs00174379_m1) and human *18S* rRNA (Hs99999901_s1) were purchased from Thermo Fisher Scientific. SYRB green primers for mouse *Th* gene (Mm.PY.58.33106186), mouse *Drd1* (Mm.PT.58.43576955.g), *Drd2* (Mm.PT.58.7811767), *Drd3* (Mm.PT.58.12468013), *Drd4* (Mm.PT.58.10440082) and *Drd5* (Mm.PT.58.43058779.g) were purchased from Integrated DNA Technologies. Relative gene expression was measured by normalizing to *18S* rRNA using

Ct (cycle threshold difference). Expression of *Il4*, *Il5*, *Il13* and *Areg* in ILCs was normalized to the housekeeping gene *Actb* (Thermo Fisher Scientific, 4352341E).

Western Blot.—Lungs and cells were homogenized in RIPA buffer with cOmplete™proteinase inhibitor cocktail (Roche, 11697498001) followed by standard Western blot assays. Primary antibodies include rabbit anti-tyrosine hydroxylase (1:1000; EMD Millipore, AB152), rabbit anti-DBH (1:1000; EMD Millipore, AB1585), rabbit anti-VAChT (1:1000; Abcam, AB68986), rabbit anti-CGRP (1:1000; Sigma Aldrich, C8198), mouse anti-p-STAT6 (pY641) (1:1000; BD Biosciences, 558241), rabbit anti-DRD4 (1:1000; Sigma Aldrich, SAB4500672-100UG), mouse anti-DRD4 (1:1000; EMD Millipore, MABN125) and mouse anti-β-actin (1:3000; Sigma Aldrich, A5441). HRP-conjugated secondary antibodies include: goat anti-rabbit (1:3000; Santa Cruz Biotechnology, sc-2004) and goat anti-mouse (1:3000; BD Biosciences, 554002). The antigen-antibody complex was detected by SuperSignal™ West Pico PLUS Chemiluminescent Substrate (Thermo Fisher, 34577).

ELISAs.—Serum was collected from blood samples of mice and the amount of OVA-specific IgE and total IgE were analyzed using ELISA Kits (BioLegend, 439807 and eBioscience, 88-50460-88). BALF was collected and the amount of IL-4, IL-5 and IL-13 were analyzed using Ready-Set-Go! ELISA sets (eBioscience, 88-7044-86, 88-7054-88 and 88-7137-76). For dopamine and norepinephrine assays, the lung was homogenized in cold RIPA buffer (Thermo Scientific, PI89900) and the amount of dopamine and norepinephrine in the supernatant were analyzed by ELISA kits (Abnova, 89-028-620 and 89-028-610). For the measurement of intracellular cAMP, naïve $CD4^+$ T cells were cultured under Th0 condition overnight followed by the treatment with dopamine (10 μM) and forskolin (1 μM) for 1 hr. Cells were lysed with 100 μL RIPA buffer with 1 mM phenylmethylsulfonyl fluoride. The supernatant was collected before assays using the cAMP XP® Assay Kit (Cell signaling, 4339S).

RNA-seq analyses.—Naïve mouse $CD4^+$ T cells in Th0 culture with and without dopamine treatment were harvested on day 4. Total RNA was purified with a RNeasy kit (Qiagen) followed with DNase I treatment. RNA-seq libraries were prepared with the TruSeq Stranded Total RNA with Ribo-Zero Globin kit (Illumina) following the manufacturer's instructions. Quality of the libraries was validated by quantitation with picogreen, size analysis on an Agilent Bioanalyzer or Tapestation 2200 and qPCR quantitation against a standard curve. Bar-coded cDNA libraries were pooled together in equal concentrations in one pool per biological triplicates and were sequenced on a HiSeq2500 (Illumina) at the Translational Genomics Core of Partners HealthCare Personalized Medicine (Cambridge, MA, USA). Briefly, raw reads were pre-processed using FastQC v.0.11.2, and then mapped to the mouse genome (Mus musculus UCSC version mm10) using the TopHat version 2.0.13. The read count table was produced using HTSeq v. 0.6. Differentially expressed gene transcripts were selected based on an adjusted p-value less than 0.05. Heatmap and volcano plot were performed using R-3.2.5. For pathway analysis, a list of all genes detected in the samples was ranked on the t-statistic. This list was analyzed with the fGSEA package in R using the complete Molecular Signatures Database MSigDB

v6.1 gene set (http://software.broadinstitute.org/gsea/index.jsp). We only showed those pathways that had an FDR < 0.05.

Quantitative Chromatin precipitation (ChIP)-qPCR.—Cultures of naïve $CD4^+$ T cells were harvested on day 4. Histone was cross-linked to DNA with 1% paraformaldehyde in PBS for 10 minutes at 37°C. After washing with cold PBS, cells were re-suspended in 100 μL SDS lysis buffer per 1 million cells that contained 1% SDS, 10mM EDTA, 50mM Tris-HCl (pH 8.1) and cOmplete™proteinase inhibitor cocktail. Cells in suspension were sonicated using QSONICA Model Q125(50A with 14 cycles of 30s on and 30s off) to break genomic DNA into fragments between 200-500 bp in length. 100 μL of each sample was used as template for measurement of input DNA. Another 100 μL of each sample was diluted with 900 μL of ChIP dilution buffer (0.01% SDS, 1.1% Triton X-100, 1.2 mM EDTA, 16.7 mM Tris-HCl (pH 8.1), 150mM NaCl) and pre-cleared with 60 μL salmon sperm DNA (Invitrogen, 15632011) /protein-A agarose slurry (Thermo Fisher, 20421) for 1 h at 4°C with rotation. After centrifugation, pre-cleared samples were incubated with 5 μg of anti-trimethyl-Histone H3 (Lys27) antibody (Millipore, 07-449) overnight at 4°C with rotation followed by 2 hr incubation with protein A agarose slurry pretreated with salmon sperm DNA. The beads were then pelleted and washed extensively using buffers with increasing concentrations of NaCl. Immune complexes were eluted twice by addition of 250 μL of elution buffer (1% SDS, 0.1M $NaHCO_3$) and incubation for 15 minutes with rotation at room temperature. Cross-linking was reversed by adding 20 μL NaCl (5 M) and incubating at 65°C overnight. The samples were then treated with 1 μL RNase A (Qiagen, 1031301) at 37°C for 1 hr and 2 μL Proteinase K (Roche, 14164600) at 45°C for 2 hr before DNA extraction using phenol/chloroform and purified using ethanol. The primers used for ChIP q-PCR were previously described (Tumes et al., 2013) and purchased from Integrated DNA Technologies. The relative H3K27me3 binding to the target loci was measured by normalizing to the input material using Ct.

Quantification and Statistical Analyses.—Quantification and statistical analyzed were described in the Methods section above and Figure legends associated with each experiment. GraphPad Prism 6 was used for data analysis. Data in all bar graphs represent mean ± SEM from at least 3 independent experiments. For comparisons between two conditions, statistical significance was analyzed using the unpaired Student's t test. For multiple comparisons between treatment and methacholine concentration or genotype (Figures 5H, S5K and S6J), statistical analysis was performed with one-way ANOVA followed by Tukey's posthoc test for multiple comparisons. The difference between experimental groups was considered statistically significant if P value was less than 0.05.

DATA AND CODE AVAILABILITY

The RNA-seq datasets of Th0 cultures with and without dopamine treatment are generated during this study and are available at the GEO repository with the accession number GSE137968.

Supplementary Material

Refer to Web version on PubMed Central for supplementary material.

Acknowledgments

References

Aki D, Li H, Zhang W, Zheng M, Elly C, Lee JH, Zou W, and Liu YC (2018). The E3 ligases Itch and WWP2 cooperate to limit TH2 differentiation by enhancing signaling through the TCR. Nature immunology 19, 766–775. [PubMed: 29925997]

Anastassiou ED, Paliogianni F, Balow JP, Yamada H, and Boumpas DT (1992). Prostaglandin E2 and other cyclic AMP-elevating agents modulate IL-2 and IL-2R alpha gene expression at multiple levels. Journal of immunology 148, 2845–2852.

Anders S, Pyl PT, and Huber W (2015). HTSeq--a Python framework to work with high-throughput sequencing data. Bioinformatics 31, 166–169. [PubMed: 25260700]

Angeletti PU, and Levi-Montalcini R (1972). Growth inhibition of sympathetic cells by some adrenergic blocking agents (6-hydroxydopamine-mice and rats-immunosympathectomy-chemical sympathectomy-superior cervical ganglion). Proceedings of the National Academy of Sciences of the United States of America 69, 86–88. [PubMed: 4333047]

Aven L, and Ai X (2013). Mechanisms of respiratory innervation during embryonic development. Organogenesis 9, 194–198. [PubMed: 23974176]

Aven L, Paez-Cortez J, Achey R, Krishnan R, Ram-Mohan S, Cruikshank WW, Fine A, and Ai X (2014). An NT4/TrkB-dependent increase in innervation links early-life allergen exposure to persistent airway hyperreactivity. FASEB journal : official publication of the Federation of American Societies for Experimental Biology 28, 897–907. [PubMed: 24221086]

Barbacid M (1994). The Trk family of neurotrophin receptors. Journal of neurobiology 25, 1386–1403. [PubMed: 7852993]

Barrios J, Patel KR, Aven L, Achey R, Minns MS, Lee Y, Trinkaus-Randall VE, and Ai X (2017). Early life allergen-induced mucus overproduction requires augmented neural stimulation of pulmonary neuroendocrine cell secretion. FASEB journal : official publication of the Federation of American Societies for Experimental Biology 31, 4117–4128. [PubMed: 28566470]

Beaulieu JM, and Gainetdinov RR (2011). The physiology, signaling, and pharmacology of dopamine receptors. Pharmacol Rev 63, 182–217. [PubMed: 21303898]

Becerra-Diaz M, Wills-Karp M, and Heller NM (2017). New perspectives on the regulation of type II inflammation in asthma. F1000Research 6, 1014. [PubMed: 28721208]

Bergquist J, and Silberring J (1998). Identification of catecholamines in the immune system by electrospray ionization mass spectrometry. Rapid communications in mass spectrometry : RCM 12, 683–688. [PubMed: 9633115]

Borovikova LV, Ivanova S, Zhang M, Yang H, Botchkina GI, Watkins LR, Wang H, Abumrad N, Eaton JW, and Tracey KJ (2000). Vagus nerve stimulation attenuates the systemic inflammatory response to endotoxin. Nature 405, 458–462. [PubMed: 10839541]

Bourne JA (2001). SCH 23390: the first selective dopamine D1-like receptor antagonist. CNS Drug Rev 7, 399–414. [PubMed: 11830757]

Buttari B, Profumo E, Domenici G, Tagliani A, Ippoliti F, Bonini S, Businaro R, Elenkov I, and Rigano R (2014). Neuropeptide Y induces potent migration of human immature dendritic cells and promotes a Th2 polarization. FASEB journal : official publication of the Federation of American Societies for Experimental Biology 28, 3038–3049. [PubMed: 24699455]

Cardoso V, Chesne J, Ribeiro H, Garcia-Cassani B, Carvalho T, Bouchery T, Shah K, Barbosa-Morais NL, Harris N, and Veiga-Fernandes H (2017). Neuronal regulation of type 2 innate lymphoid cells via neuromedin U. Nature 549, 277–281. [PubMed: 28869974]

Chavan SS, Pavlov VA, and Tracey KJ (2017). Mechanisms and Therapeutic Relevance of Neuro-immune Communication. Immunity 46, 927–942. [PubMed: 28636960]

Chen T, Tibbitt CA, Feng X, Stark JM, Rohrbeck L, Rausch L, Sedimbi SK, Karlsson MCI, Lambrecht BN, Karlsson Hedestam GB, et al. (2017). PPAR-gamma promotes type 2 immune responses in allergy and nematode infection. Science immunology 2.

Church RJ, Jania LA, and Koller BH (2012). Prostaglandin E(2) produced by the lung augments the effector phase of allergic inflammation. Journal of immunology 188, 4093–4102.

Cohen L, E X, Tarsi J, Ramkumar T, Horiuchi TK, Cochran R, DeMartino S, Schechtman KB, Hussain I, Holtzman MJ, et al. (2007). Epithelial cell proliferation contributes to airway remodeling in severe asthma. American journal of respiratory and critical care medicine 176, 138–145. [PubMed: 17463414]

Contreras F, Prado C, Gonzalez H, Franz D, Osorio-Barrios F, Osorio F, Ugalde V, Lopez E, Elgueta D, Figueroa A, et al. (2016). Dopamine Receptor D3 Signaling on CD4+ T Cells Favors Th1- and Th17-Mediated Immunity. Journal of immunology 196, 4143–4149.

Cosentino M, Fietta AM, Ferrari M, Rasini E, Bombelli R, Carcano E, Saporiti F, Meloni F, Marino F, and Lecchini S (2007). Human CD4+CD25+ regulatory T cells selectively express tyrosine hydroxylase and contain endogenous catecholamines subserving an autocrine/paracrine inhibitory functional loop. Blood 109, 632–642. [PubMed: 16985181]

Cote-Sierra J, Foucras G, Guo L, Chiodetti L, Young HA, Hu-Li J, Zhu J, and Paul WE (2004). Interleukin 2 plays a central role in Th2 differentiation. Proceedings of the National Academy of Sciences of the United States of America 101, 3880–3885. [PubMed: 15004274]

de Kleer IM, Kool M, de Bruijn MJ, Willart M, van Moorleghem J, Schuijs MJ, Plantinga M, Beyaert R, Hams E, Fallon PG, et al. (2016). Perinatal Activation of the Interleukin-33 Pathway Promotes Type 2 Immunity in the Developing Lung. Immunity 45, 1285–1298. [PubMed: 27939673]

Dettman EJ, Simko SJ, Ayanga B, Carofino BL, Margolin JF, Morse HC 3rd, and Justice MJ (2011). Prdm14 initiates lymphoblastic leukemia after expanding a population of cells resembling common lymphoid progenitors. Oncogene 30, 2859–2873. [PubMed: 21339739]

Fahy JV (2015). Type 2 inflammation in asthma--present in most, absent in many. Nature reviews Immunology 15, 57–65.

Felten DL, Felten SY, Carlson SL, Olschowka JA, and Livnat S (1985). Noradrenergic and peptidergic innervation of lymphoid tissue. Journal of immunology 135, 755s–765s.

Ferreira MA, Vonk JM, Baurecht H, Marenholz I, Tian C, Hoffman JD, Helmer Q, Tillander A, Ullemar V, van Dongen J, et al. (2017). Shared genetic origin of asthma, hay fever and eczema elucidates allergic disease biology. Nat Genet 49, 1752–1757. [PubMed: 29083406]

Flierl MA, Rittirsch D, Nadeau BA, Chen AJ, Sarma JV, Zetoune FS, McGuire SR, List RP, Day DE, Hoesel LM, et al. (2007). Phagocyte-derived catecholamines enhance acute inflammatory injury. Nature 449, 721–725. [PubMed: 17914358]

Franz D, Contreras F, Gonzalez H, Prado C, Elgueta D, Figueroa C, and Pacheco R (2015). Dopamine receptors D3 and D5 regulate CD4(+)T-cell activation and differentiation by modulating ERK activation and cAMP production. J Neuroimmunol 284, 18–29. [PubMed: 26025054]

Goto Y, Otani S, and Grace AA (2007). The Yin and Yang of dopamine release: a new perspective. Neuropharmacology 53, 583–587. [PubMed: 17709119]

Hebel K, Weinert S, Kuropka B, Knolle J, Kosak B, Jorch G, Arens C, Krause E, Braun-Dullaeus RC, and Brunner-Weinzierl MC (2014). CD4+ T cells from human neonates and infants are poised spontaneously to run a nonclassical IL-4 program. Journal of immunology 192, 5160–5170.

Henriksson J, Chen X, Gomes T, Ullah U, Meyer KB, Miragaia R, Duddy G, Pramanik J, Yusa K, Lahesmaa R, et al. (2019). Genome-wide CRISPR Screens in T Helper Cells Reveal Pervasive Crosstalk between Activation and Differentiation. Cell 176, 882–896 e818. [PubMed: 30639098]

Ho IC, Lo D, and Glimcher LH (1998). c-maf promotes T helper cell type 2 (Th2) and attenuates Th1 differentiation by both interleukin 4-dependent and -independent mechanisms. The Journal of experimental medicine 188, 1859–1866. [PubMed: 9815263]

Huang Y, Qiu AW, Peng YP, Liu Y, Huang HW, and Qiu YH (2010). Roles of dopamine receptor subtypes in mediating modulation of T lymphocyte function. Neuro Endocrinol Lett 31, 782–791. [PubMed: 21196914]

Hyttel J (1983). SCH 23390 - the first selective dopamine D-1 antagonist. European journal of pharmacology 91, 153–154. [PubMed: 6225651]

Ilani T, Strous RD, and Fuchs S (2004). Dopaminergic regulation of immune cells via D3 dopamine receptor: a pathway mediated by activated T cells. FASEB journal : official publication of the Federation of American Societies for Experimental Biology 18, 1600–1602. [PubMed: 15319371]

Josefsson E, Bergquist J, Ekman R, and Tarkowski A (1996). Catecholamines are synthesized by mouse lymphocytes and regulate function of these cells by induction of apoptosis. Immunology 88, 140–146. [PubMed: 8707341]

Kim MN, Hong JY, Shim DH, Sol IS, Kim YS, Lee JH, Kim KW, Lee JM, and Sohn MH (2018). Activated Leukocyte Cell Adhesion Molecule Stimulates the T-Cell Response in Allergic Asthma. American journal of respiratory and critical care medicine 197, 994–1008. [PubMed: 29394080]

Klose CSN, Mahlakoiv T, Moeller JB, Rankin LC, Flamar AL, Kabata H, Monticelli LA, Moriyama S, Putzel GG, Rakhilin N, et al. (2017). The neuropeptide neuromedin U stimulates innate lymphoid cells and type 2 inflammation. Nature 549, 282–286. [PubMed: 28869965]

Kustrimovic N, Rasini E, Legnaro M, Marino F, and Cosentino M (2014). Expression of dopaminergic receptors on human CD4+ T lymphocytes: flow cytometric analysis of naive and memory subsets and relevance for the neuroimmunology of neurodegenerative disease. J Neuroimmune Pharmacol 9, 302–312. [PubMed: 24682738]

Le Gros G, Ben-Sasson SZ, Seder R, Finkelman FD, and Paul WE (1990). Generation of interleukin 4 (IL-4)-producing cells in vivo and in vitro: IL-2 and IL-4 are required for in vitro generation of IL-4-producing cells. The Journal of experimental medicine 172, 921–929. [PubMed: 2117636]

Margueron R, and Reinberg D (2011). The Polycomb complex PRC2 and its mark in life. Nature 469, 343–349. [PubMed: 21248841]

Moreland RB, Patel M, Hsieh GC, Wetter JM, Marsh K, and Brioni JD (2005). A-412997 is a selective dopamine D4 receptor agonist in rats. Pharmacology, biochemistry, and behavior 82, 140–147.

Mori T, Kabashima K, Fukamachi S, Kuroda E, Sakabe J, Kobayashi M, Nakajima S, Nakano K, Tanaka Y, Matsushita S, et al. (2013). D1-like dopamine receptors antagonist inhibits cutaneous immune reactions mediated by Th2 and mast cells. J Dermatol Sci 71, 37–44. [PubMed: 23639699]

Moriyama S, Brestoff JR, Flamar AL, Moeller JB, Klose CSN, Rankin LC, Yudanin NA, Monticelli LA, Putzel GG, Rodewald HR, et al. (2018). beta2-adrenergic receptor-mediated negative regulation of group 2 innate lymphoid cell responses. Science 359, 1056–1061. [PubMed: 29496881]

Muller J, Sperl B, Reindl W, Kiessling A, and Berg T (2008). Discovery of chromone-based inhibitors of the transcription factor STAT5. Chembiochem : a European journal of chemical biology 9, 723–727. [PubMed: 18247434]

Nakano K, Higashi T, Takagi R, Hashimoto K, Tanaka Y, and Matsushita S (2009). Dopamine released by dendritic cells polarizes Th2 differentiation. Int Immunol 21, 645–654. [PubMed: 19332443]

Ogren SO, Hall H, Kohler C, Magnusson O, and Sjostrand SE (1986). The selective dopamine D2 receptor antagonist raclopride discriminates between dopamine-mediated motor functions. Psychopharmacology 90, 287–294. [PubMed: 2947255]

Ohtake J, Kaneumi S, Tanino M, Kishikawa T, Terada S, Sumida K, Masuko K, Ohno Y, Kita T, Iwabuchi S, et al. (2015). Neuropeptide signaling through neurokinin-1 and neurokinin-2 receptors augments antigen presentation by human dendritic cells. The Journal of allergy and clinical immunology 136, 1690–1694. [PubMed: 26371842]

Papa I, Saliba D, Ponzoni M, Bustamante S, Canete PF, Gonzalez-Figueroa P, McNamara HA, Valvo S, Grimbaldeston M, Sweet RA, et al. (2017). TFH-derived dopamine accelerates productive synapses in germinal centres. Nature 547, 318–323. [PubMed: 28700579]

Patel KR, Aven L, Shao F, Krishnamoorthy N, Duvall MG, Levy BD, and Ai X (2016). Mast cell-derived neurotrophin 4 mediates allergen-induced airway hyperinnervation in early life. Mucosal immunology 9, 1466–1476. [PubMed: 26860818]

Patel S, Freedman S, Chapman KL, Emms F, Fletcher AE, Knowles M, Marwood R, McAllister G, Myers J, Curtis N, et al. (1997). Biological profile of L-745,870, a selective antagonist with high affinity for the dopamine D4 receptor. The Journal of pharmacology and experimental therapeutics 283, 636–647. [PubMed: 9353380]

Radzikinas K, Aven L, Jiang Z, Tran T, Paez-Cortez J, Boppidi K, Lu J, Fine A, and Ai X (2011). A Shh/miR-206/BDNF cascade coordinates innervation and formation of airway smooth muscle. The Journal of neuroscience : the official journal of the Society for Neuroscience 31, 15407–15415. [PubMed: 22031887]

Rubinstein M, Phillips TJ, Bunzow JR, Falzone TL, Dziewczapolski G, Zhang G, Fang Y, Larson JL, McDougall JA, Chester JA, et al. (1997). Mice lacking dopamine D4 receptors are supersensitive to ethanol, cocaine, and methamphetamine. Cell 90, 991–1001. [PubMed: 9323127]

Sarkar C, Das S, Chakroborty D, Chowdhury UR, Basu B, Dasgupta PS, and Basu S (2006). Cutting Edge: Stimulation of dopamine D4 receptors induce T cell quiescence by up-regulating Kruppel-like factor-2 expression through inhibition of ERK1/ERK2 phosphorylation. Journal of immunology 177, 7525–7529.

Sherrill JD, Gao PS, Stucke EM, Blanchard C, Collins MH, Putnam PE, Franciosi JP, Kushner JP, Abonia JP, Assa'ad AH, et al. (2010). Variants of thymic stromal lymphopoietin and its receptor associate with eosinophilic esophagitis. The Journal of allergy and clinical immunology 126, 160–165 e163. [PubMed: 20620568]

Stern DA, Morgan WJ, Halonen M, Wright AL, and Martinez FD (2008). Wheezing and bronchial hyper-responsiveness in early childhood as predictors of newly diagnosed asthma in early adulthood: a longitudinal birth-cohort study. Lancet 372, 1058–1064. [PubMed: 18805334]

Talbot S, Abdulnour RE, Burkett PR, Lee S, Cronin SJ, Pascal MA, Laedermann C, Foster SL, Tran JV, Lai N, et al. (2015). Silencing Nociceptor Neurons Reduces Allergic Airway Inflammation. Neuron 87, 341–354. [PubMed: 26119026]

Tortorolo L, Langer A, Polidori G, Vento G, Stampachiacchere B, Aloe L, and Piedimonte G (2005). Neurotrophin overexpression in lower airways of infants with respiratory syncytial virus infection. American journal of respiratory and critical care medicine 172, 233–237. [PubMed: 15879412]

Tuck ML (1986). The sympathetic nervous system in essential hypertension. American heart journal 112, 877–886. [PubMed: 3532745]

Tumes DJ, Onodera A, Suzuki A, Shinoda K, Endo Y, Iwamura C, Hosokawa H, Koseki H, Tokoyoda K, Suzuki Y, et al. (2013). The polycomb protein Ezh2 regulates differentiation and plasticity of CD4(+) T helper type 1 and type 2 cells. Immunity 39, 819–832. [PubMed: 24238339]

Van Dyken SJ, Nussbaum JC, Lee J, Molofsky AB, Liang HE, Pollack JL, Gate RE, Haliburton GE, Ye CJ, Marson A, et al. (2016). A tissue checkpoint regulates type 2 immunity. Nature immunology 17, 1381–1387. [PubMed: 27749840]

Verjans E, Ohl K, Reiss LK, van Wijk F, Toncheva AA, Wiener A, Yu Y, Rieg AD, Gaertner VD, Roth J, et al. (2015). The cAMP response element modulator (CREM) regulates TH2 mediated inflammation. Oncotarget 6, 38538–38551. [PubMed: 26459392]

Wang H, Yu M, Ochani M, Amella CA, Tanovic M, Susarla S, Li JH, Wang H, Yang H, Ulloa L, et al. (2003). Nicotinic acetylcholine receptor alpha7 subunit is an essential regulator of inflammation. Nature 421, 384–388. [PubMed: 12508119]

Watanabe T, Fajt ML, Trudeau JB, Voraphani N, Hu H, Zhou X, Holguin F, and Wenzel SE (2015). Brain-Derived Neurotrophic Factor Expression in Asthma. Association with Severity and Type 2 Inflammatory Processes. American journal of respiratory cell and molecular biology 53, 844–852. [PubMed: 25945802]

Zheng W, and Flavell RA (1997). The transcription factor GATA-3 is necessary and sufficient for Th2 cytokine gene expression in CD4 T cells. Cell 89, 587–596. [PubMed: 9160750]

Zhu J, Cote-Sierra J, Guo L, and Paul WE (2003). Stat5 activation plays a critical role in Th2 differentiation. Immunity 19, 739–748. [PubMed: 14614860]

Highlights

- Sympathetic innervation in the lung undergoes a dopaminergic-to-adrenergic transition

- Dopamine signals through DRD4 in CD4$^+$ T cells to induce a Th2 phenotype

- Dopaminergic nerves in the early lung foster susceptibility to allergic inflammation
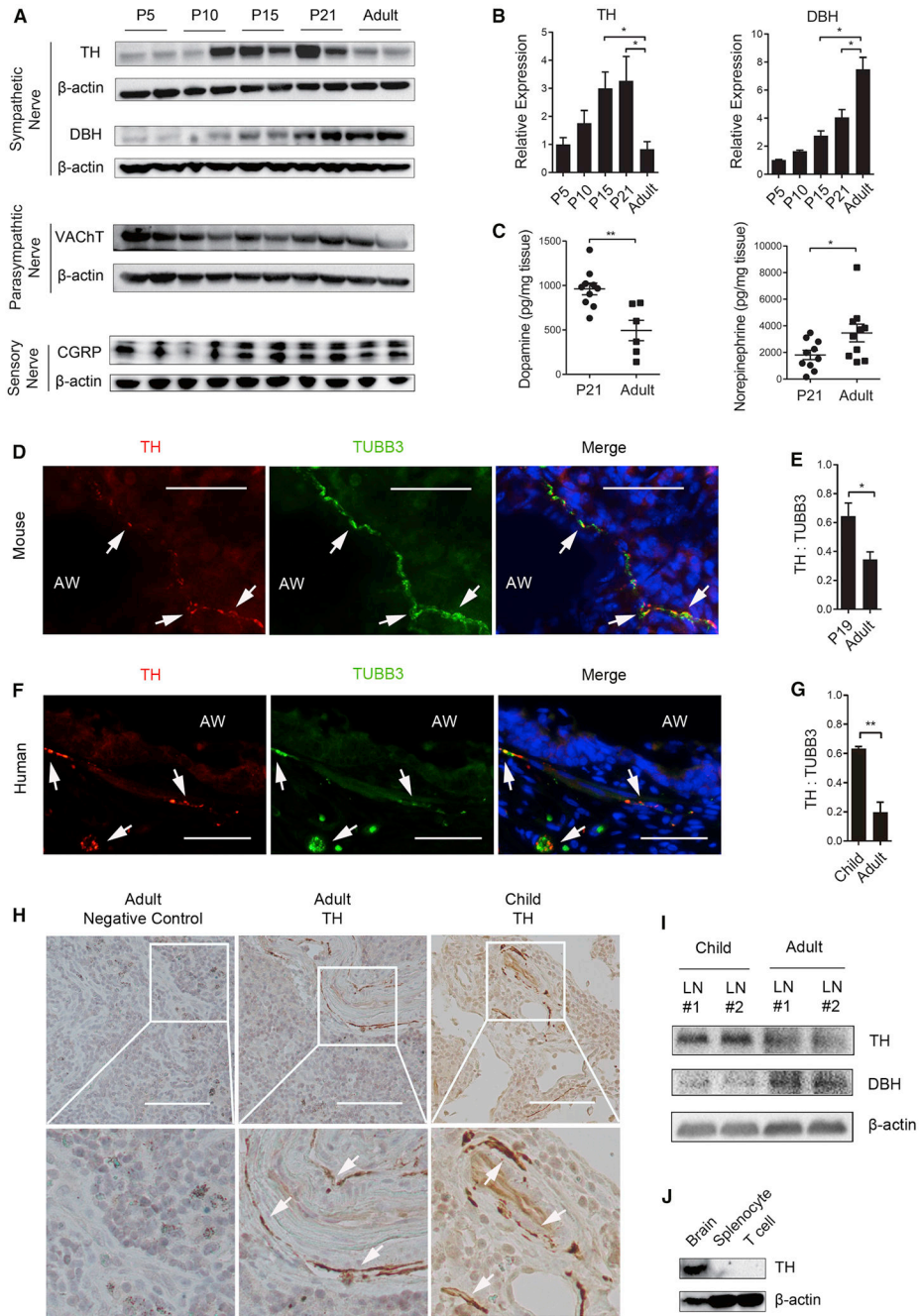
Figure 1. Sympathetic nerves in the lung transition from dopaminergic to adrenergic phenotypes from early life to adult life.
(**A**) Western blot analyses of the markers of sympathetic nerves (tyrosine hydroxylase (TH) and dopamine β-hydroxylase (DBH)), parasympathetic nerves (vesicular acetylcholine transporter, VAChT) and sensory nerves (calcitonin gene related peptide, CGRP) in mouse lungs at different postnatal ages. β-actin was loading control. Each lane represents one sample. The expression of TH and DBH is presented as fold change relative to postnatal day 5 (P5) in (**B**). N=6 from 2 independent experiments. (**C**) The amount of dopamine and norepinephrine in the lung of P21 and adult mice. Results were normalized to the lung

weight. Each mark represents one sample. (**D**, **F**) Double fluorescent staining for TH and neuron-specific class III β-tubulin (TUBB3) in the lung of mice and humans. To visualize nerves, frozen sections (15 μm in thickness) were used for double staining. Nuclei were labelled with Hoechst dye. Arrows mark TH+TUBB3+ nerves. AW, airway. Scale bars, 30 μm. (**E**, **G**) Relative abundance of TH+ nerves in the lung of mice and humans of two age groups. For quantification, the immunoreactivity of TH was normalized to TUBB3 in double-stained tissue sections. Airways with a diameter of 0.2-0.5 mm in P19 and adult mice and human mid-sized airways with a diameter of 1-2 mm in children (0-13 years of age) and adults (40-65 years of age) were quantified. Data represent mean ± SEM from 5 non-overlapping images from each sample and a total of 3 mouse samples and 4 human samples of each age group. (**H**) Representative images of TH staining of lymph nodes associated with donor lungs. Bottom panels are enlarged images outlined in top panels. Arrows point to TH+ nerves. Similar results were obtained from 3 donors for each age group. (**I**) The expression of TH and DBH in human lymph nodes of each age group assayed by Western blot (See also Figure S1). (**J**) The amount of TH in mouse brain, splenocytes and purified CD4+ T cells assayed by Western blot. Data represent the results from 3 independent experiments. *p<0.05 and **p<0.01 by two-tailed Student's t test. See also Figure S1.
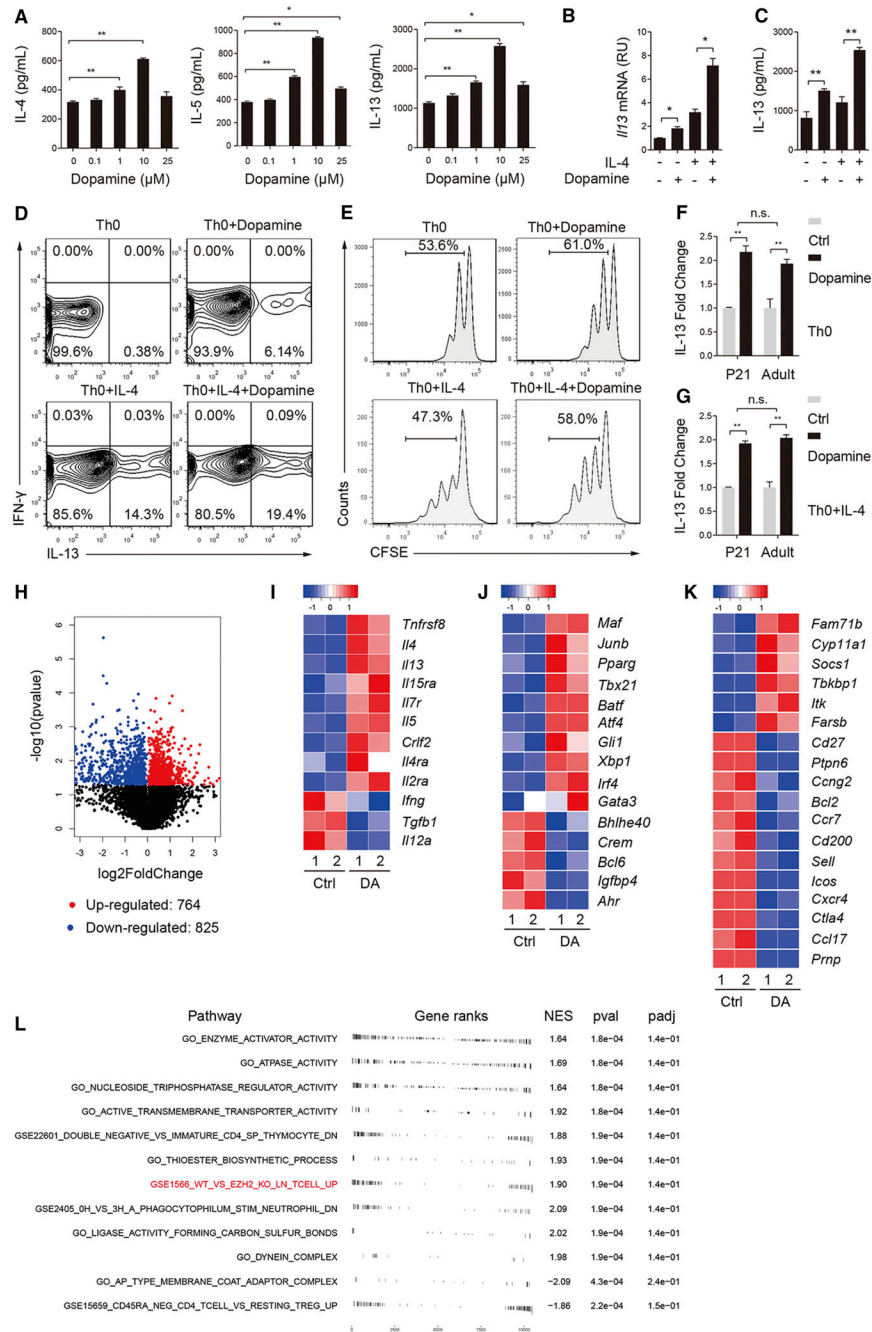
Figure 2. Dopamine promotes a Th2 phenotype in naïve CD4+ T cell cultures.
Naïve CD4+ T cells isolated from mouse spleens were stimulated with αCD3 and αCD28 (Th0) and with IL-4 (Th0+IL-4). Cultures were analyzed at day 4. Except for (**A**), all other cultures were treated with 10 μM dopamine. (**A**) Production of IL-4, IL-5 and IL-13 by Th0 cultures treated with increasing concentrations of dopamine. Data represent mean ± SEM of 3 independent experiments. (**B, C**) *Il13* mRNA and protein expression in cultures with and without dopamine and IL-4 (10 ng/mL). Data are representative of at least 5 independent experiments. (**D**) Flow cytometry analyses of CD4+ T cell cultures for IL-13 and IFN-γ expression. Data are representative of 2 independent experiments. (**E**) Flow cytometry

analyses of cell proliferation in each culture condition. Data are representative of 3 independent experiments. (**F, G**) IL-13 production in dopamine-treated, neonatal and adult cultures relative to untreated baseline control. Data represents mean ± SEM from 3 independent experiments. (**H**) Volcano plot of transcripts with FPKM>1 in RNA sequencing of Th0 cultures with and without dopamine. Red dots represent significantly up-regulated genes and blue dots represent significantly down-regulated genes. (**I-K**) Heatmaps of differential gene expression of cytokines and receptors (**I**), transcriptional factors (**J**) and other genes involved in T cell activation and Th2 differentiation (**K**). Each column represents one sample. Genes were ranked by fold change. All the listed genes have an adjusted p-value < 0.05. DA, dopamine. (**L**) Pathway analyses of gene set enrichment in dopamine-treated Th0 cultures. Pathways that had an FDR < 0.05 are shown. NES = normalized enrichment score; a positive score indicates gene set enrichment at the top of the ranked list or those that were upregulated by dopamine. pval = enriched p value, and padj = Benjamini, Hochberg - adjusted p value set to < 0.25. *p<0.05 and **p<0.01 by two-tailed student's t test. See also Figure S1.
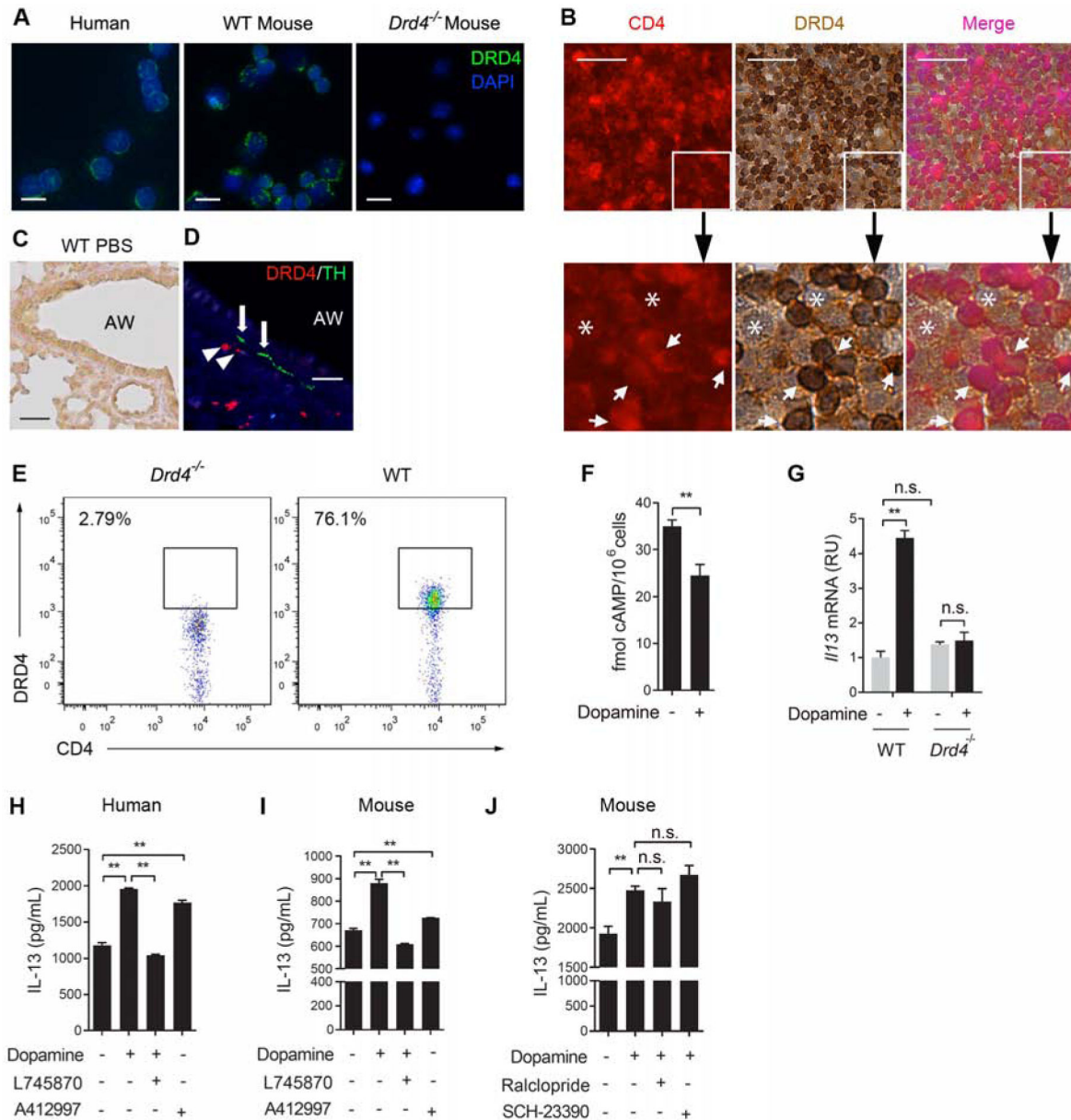
Figure 3. Dopamine signals through a major DRD4 receptor on CD4$^+$ T cells to promote the Th2 phenotype.

(**A**) Staining for DRD4 in mouse and human CD4$^+$ T cell cultures. Nuclei were labelled with Hoechst dye. (**B**) Double staining for CD4 and DRD4 using histological sections of lymph nodes associated with adult human donor lungs. The outlined area was enlarged in the bottom panel. Arrows mark CD4$^+$DRD4$^+$ cells. Asterisks mark cells that are double negative. Images are representative results in 3 donors. (**C**) DRD4 staining of lung sections of P21 mice at baseline. AW, airway. (**D**) Double staining for DRD4 and tyrosine hydroxylase (TH) in P21 mouse lungs following OVA exposure. Arrowheads mark DRD4$^+$ cells and arrows mark TH$^+$ nerves. Images in (**A-D**) are representative of the results in 3 independent experiments. (**E**) Flow cytometry analyses of DRD4 expression in CD4$^+$ T cells in mouse lungs following allergen exposure at P21. Similar results were obtained in 2

independent experiments. (**F**) The amount of intracellular cAMP in control and dopamine-treated Th0 cultures. Data represent mean ± SEM in 3 independent experiments. (**G**) *Il13* mRNA expression in wildtype and *Drd4*$^{-/-}$ CD4$^+$ T cells with or without dopamine treatment. Data represent fold change relative to WT cultures at baseline in 3 independent experiments. (**G-I**) IL-13 production by CD4$^+$ T cells in each treatment group (DRD4 antagonist L-745870 (300 nM), DRD4 agonist A412997 (100 nM), DRD2/3 antagonist raclopride (50 nM), DRD1/5 antagonist SCH-23390 (50 nM)). Data represent mean ± SEM in 3 independent experiments. **p<0.01 by two-tailed Student's t test. n.s., not significant. Scale bars, 10 μm in (**A**) and 50 μm in (**B-D**). See also Figures S2 and S3.
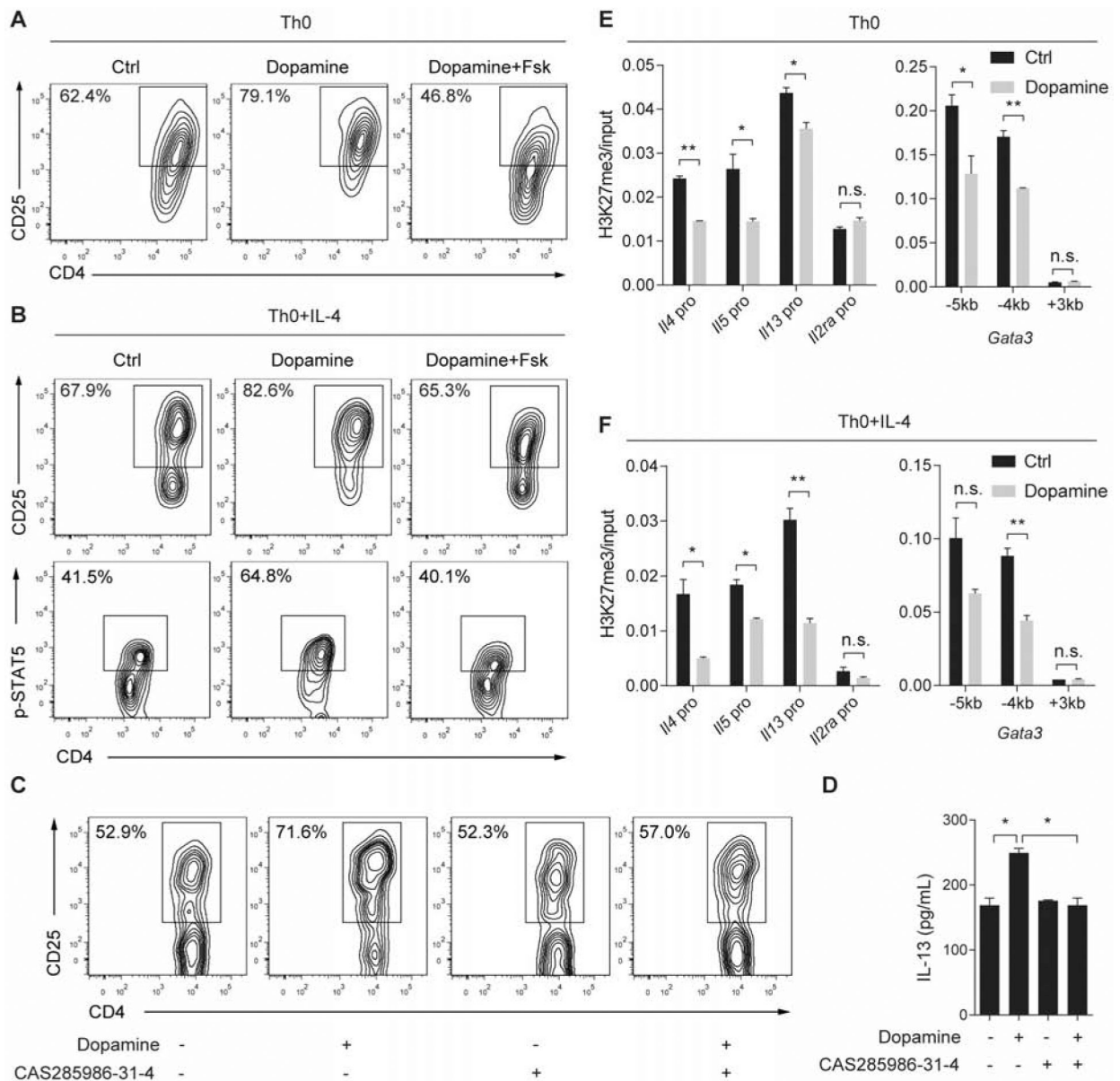
Figure 4. Dopamine promotes Th2 differentiation by upregulating IL-2 signaling and reducing H3K27me3 at Th2 gene loci.

(**A**) Flow cytometry analyses of IL-2Rα (also called CD25) in Th0 cultures treated with dopamine alone and in combination with forskolin (1 μM, Fsk). Similar results were obtained in 3 independent experiments. (**B**) Flow cytometry analyses of CD25 and p-STAT5 in Th0+IL4 cultures of each treatment group. Similar results were obtained in 5 independent experiments. (**C**) Flow cytometry analyses of CD25 expression in day 2 Th0 cultures following treatment with dopamine and a STAT5 specific inhibitor, CAS285986-31-4 (20 μM). Data are representative of 3 independent experiments. (**D**) IL-13 production in day 2 Th0 cultures in each treatment group measured by ELISA. (**E** and **F**) The relative amount of H3K27me3 at the promoter of *Il4, Il5, Il13, Il2ra* and *Gata3* genes in Th0 and Th0+IL-4 cultures by quantitative ChIP analyses. Bar graphs (**D-F**) represent mean ± SEM of three
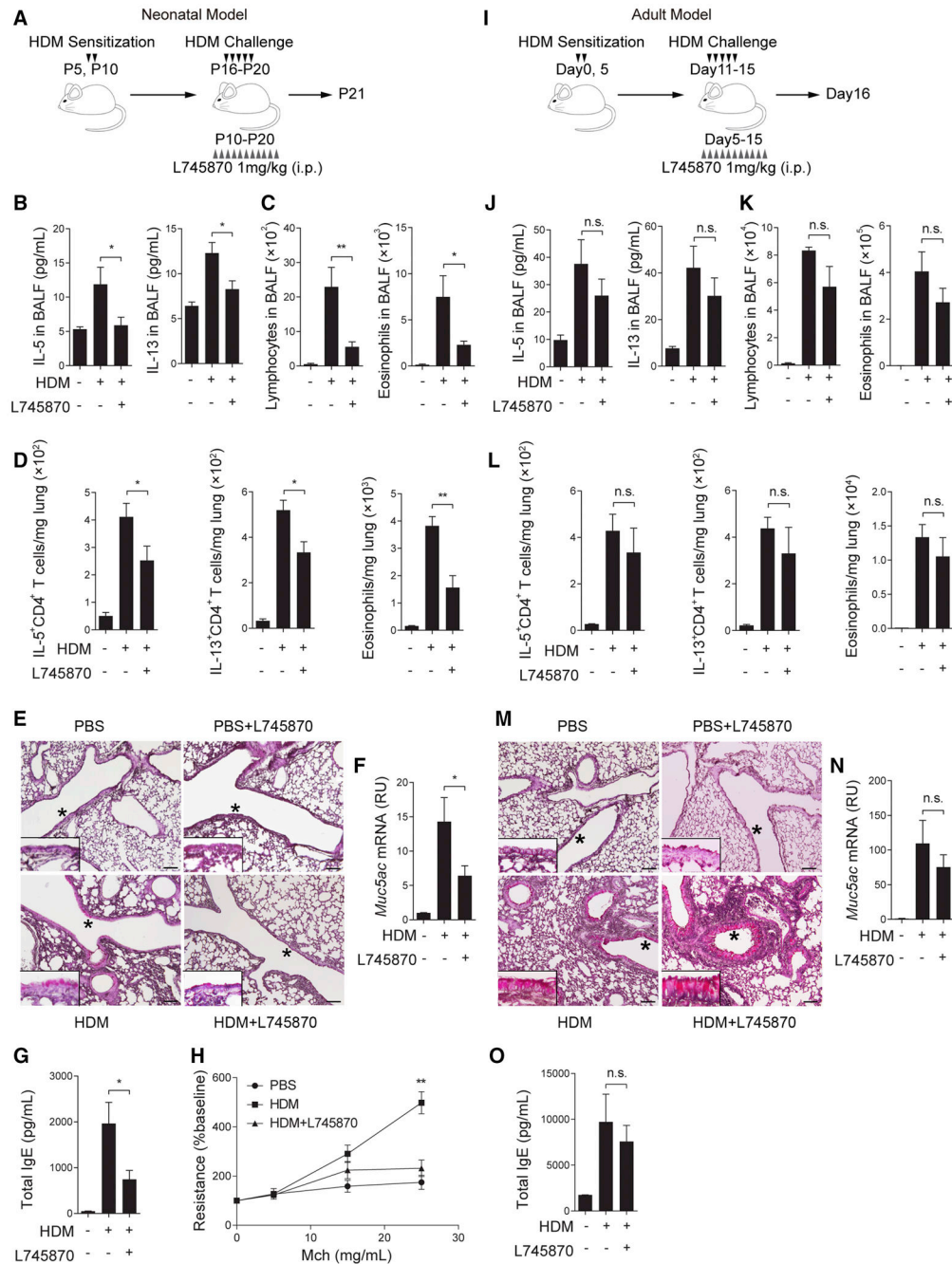
independent experiments. *p<0.05; **p<0.01 by two-tailed student's t test. See also Figure S3.

Figure 5. The dopamine-DRD4 pathway plays a significant role in Th2 inflammation in neonatal mice.

Scheme of HDM allergen sensitization and challenge with L745870 treatment in neonatal mice (**A**) and adult mice (**I**). Mice were analyzed 1 day after the last challenge. (**B** and **J**) The amount of IL-5 and IL-13 in BALF of neonatal and adult mice in each group. N=12 in 3 independent experiments in (**B**) and N=5 in 2 independent experiments in (**J**). (**C** and **K**) The abundance of lymphocytes and eosinophils in BALF of neonatal and adult mice. N=12 in 3 independent experiments in (**C**) and N=5 from 2 independent experiments in (**K**). (**D** and **L**) The abundance of IL-5^{+} and IL-13^{+}, CD4^{+} T cells and eosinophils in the lung of

neonatal and adult mice. Data were normalized to the lung weight. N=8 from 2 independent experiments in (**D**) and N=5 from 2 independent experiments in (**L**). (**E** and **M**) Representative image of PAS staining in lung sections of neonatal and adult mice. The epithelial area marked by * is enlarged and shown by the insert. Scale bars, 100 μm. (**F** and **N**) Mucus production in neonatal and adult lungs assayed by *Muc5ac* qPCR. N=12 in 3 independent experiments in (**F**) and N=5 in 2 independent experiments in (**N**). (**G** and **O**) The amount of total IgE in serum from neonatal and adult mice. N=12 in 3 independent experiments in (**G**) and N=5 in 2 independent experiments in (**O**). (**H**) Airway resistance in neonatal mice of each group relative to the baseline. N=4-5 in 2 independent experiments. **$p<0.01$ by one-way ANOVA followed by Tukey's posthoc test in (**H**). For all other panels, *$p<0.05$; **$p<0.01$ by two-tailed student's t test. n.s., not significant. See also Figures S4-S6.
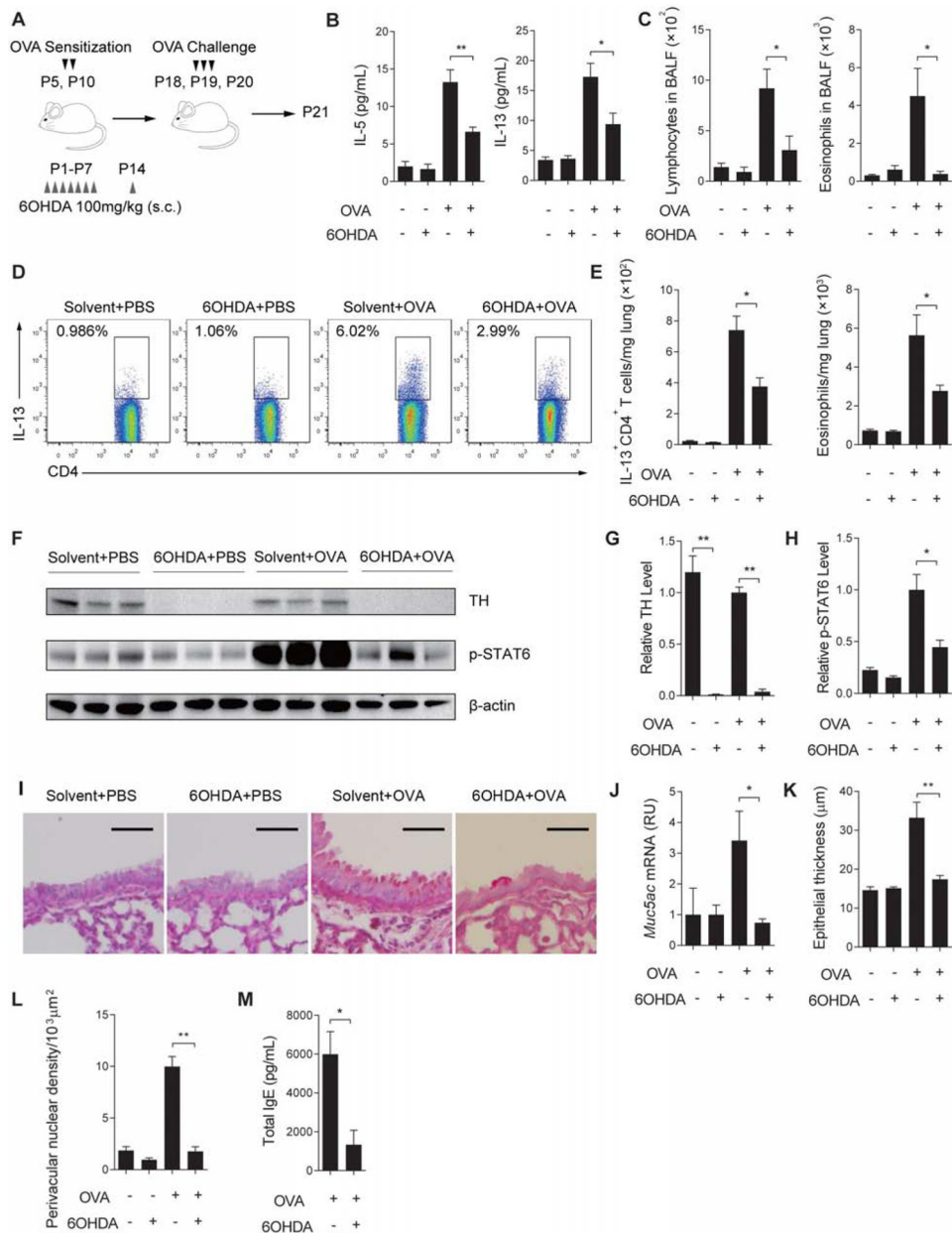
Figure 6. Ablation of dopaminergic nerves ameliorates allergic inflammation in young mice.
(**A**) Scheme of 6OHDA treatment during OVA sensitization and challenge in neonatal mice. Mice were analyzed one day after the last challenge at P21. (**B**) The amount of IL-5 and IL-13 in BALF in each group. N=5-7 in 2 independent experiments. (**C**) Quantification of lymphocytes and eosinophils in BALF at P21. N=5-7 in 2 independent experiments. (**D**) Flow cytometry analyses of IL-13$^+$CD4$^+$ T cells in the lung of each group. Similar results were obtained from 2 independent experiments. (**E**) The abundance of IL-13$^+$CD4$^+$ T cells and eosinophils in the lung of each group. Data were normalized to the lung weight. N=5-7 in 2 independent experiments. (**F-H**) Relative expression of tyrosine hydroxylase (TH) and phosphorylated STAT6 (p-STAT6) in the lung of each group by Western blot. β-actin was loading control. Each lane represents one sample. N=5-7 in 2 independent experiments. (**I**

and **J**) Mucus overproduction assayed by PAS staining and qPCR in the lung of each group. N=5 in 2 independent experiments. Scale bars, 100 μm. (**K** and **L**) Pathological assays of epithelial thickness and perivascular nuclear density. Data represent mean ± SEM of 3 non-overlapping histological areas in each mouse, 3-5 mice in each group in 2 independent experiments. (**M**) The amount of total IgE in serum from each group. N=5-7 in 2 independent experiments. *$p<0.05$ and **$p<0.01$ by two-tailed student's t test. See also Figure S7.
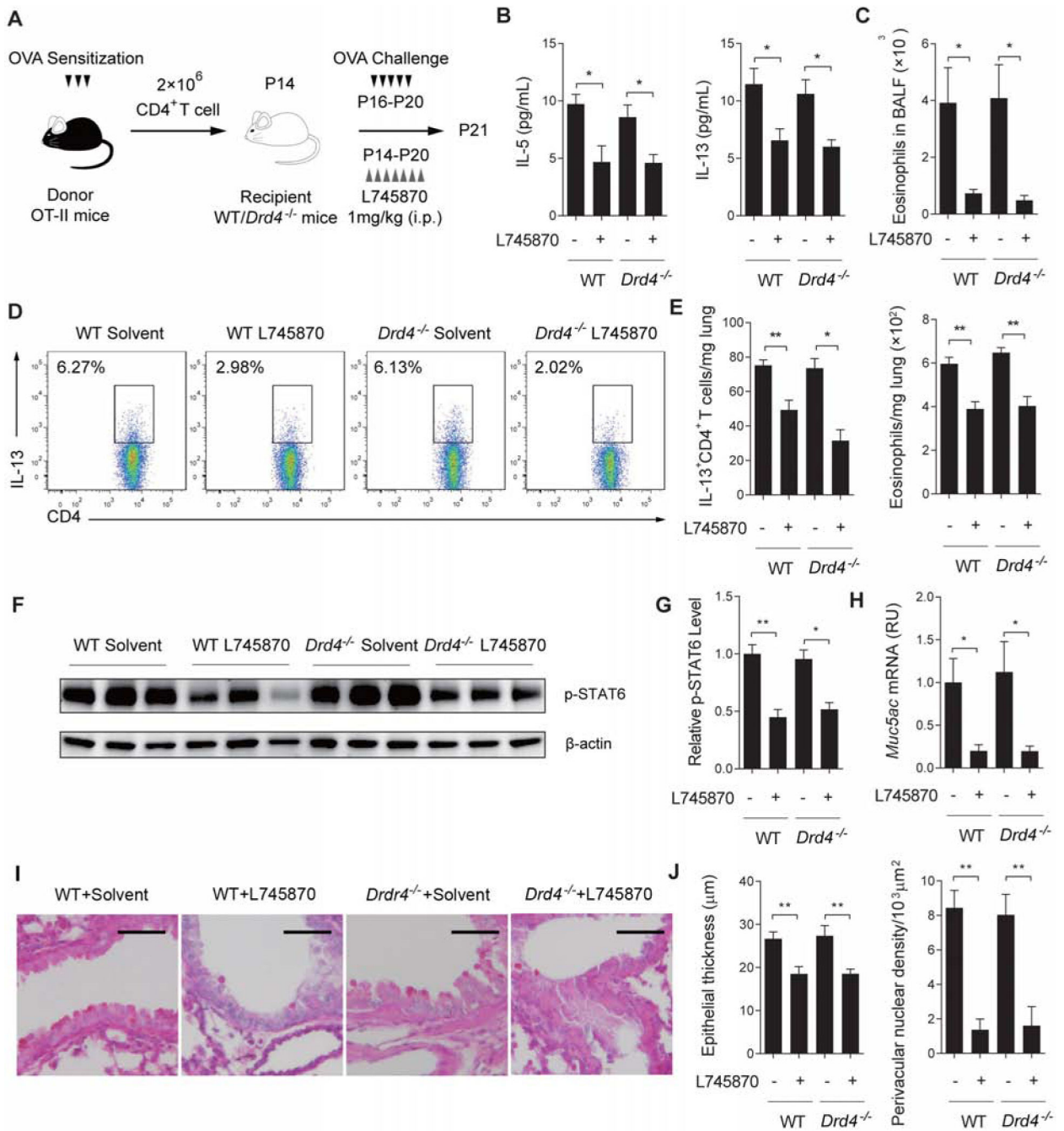
Figure 7. CD4⁺ T cells mediate dopamine signaling to promote Th2 inflammation in neonatal mice.

(**A**) Scheme of adoptive transfer of CD4⁺ OT-II cells to recipient, wildtype and *Drd4⁻/⁻* mice with and without L745870 treatment. CD4⁺ OT-II cells were isolated from OVA-sensitized donor mice at 5 weeks of age before adoptive transfer. The recipient mice were analyzed at P21. (**B**) The amount of IL-5 and IL-13 in BALF of each group. N=5-7 in 3 independent experiments. (**C**) Quantification of eosinophils in BALF of each group. N=5-7 in 3 independent experiments. (**D**) Representative flow cytometry results of IL-13⁺CD4⁺ T cells in the lung of each group. Similar results were obtained from 3 independent experiments.

(**E**) Relative abundance of IL-13$^+$CD4$^+$ T cells and eosinophils in the lung. Data were normalized to the lung weight. N=5-7 in 3 independent experiments. (**F** and **G**) The amount of p-STAT6 in the lung of each group. β-actin was loading control. N=5-7 in 3 independent experiments. (**H** and **I**) Mucus overproduction assayed by PAS staining and qPCR in the lung of each group. N=5-7 in 3 independent experiments. Scale bars, 100 μm. (**J**) Pathological assays of epithelial thickness and perivascular nuclear density. Data represent mean ± SEM of 3 non-overlapping histological areas in each mouse, 5 mice in each group in 3 independent experiments. *p<0.05 and **p<0.01 by two-tailed student's t test.

KEY RESOURCES TABLE

REAGENT or RESOURCE	SOURCE	IDENTIFIER
Antibodies		
Mouse monoclonal anti-Stat5 (Y694),FITC, clone SRBCZX	eBioscience	Cat#11-9010-41; RRID:AB_2572520
Rat monoclonal anti-MHC II, FITC, clone M5/114.15.2	eBioscience	Cat#11-5321-82; RRID:AB_465232
Armenian hamster monoclonal anti-CD3e, FITC, clone 145-2C11	eBioscience	Cat#11-0031-82; RRID:AB_464882
Rat monoclonal anti-CD62L, FITC, clone MEL-14	eBioscience	Cat#12-0621-81; RRID:AB_465720
Rat monoclonal anti-CD45, FITC, clone 30-F11	eBioscience	Cat#11-0451-82; RRID:AB_465050
Rat monoclonal anti-CD25, Alexa Fluor® 488, clone eBio3C7 (3C7)	eBioscience	Cat#53-0253-82; RRID:AB_763471
Rat monoclonal anti-CD8a, PE, clone 53-6.7	eBioscience	Cat#12-0081-83; RRID:AB_465531
Rat monoclonal anti-IL-5, PE, clone TRFK5	eBioscience	Cat#12-7052-81; RRID:AB_763588
Rat monoclonal anti-IL-13, PE, clone eBio13A	eBioscience	Cat#12-7133-41; RRID:AB_10852712
Mouse monoclonal anti-NK1.1, PE, clone PK136	eBioscience	Cat#12-5941-81; RRID:AB_466049
Rat monoclonal anti-MHC II, PE, clone M5/114.15.2	eBioscience	Cat#12-5321-81; RRID:AB_465927
Rat monoclonal anti-CD4, APC, clone RM4-5	eBioscience	Cat#17-0042-82; RRID:AB_469323
Rat monoclonal anti-CD44, APC, clone IM7	eBioscience	Cat#17-0441-81; RRID:AB_469389
Armenian hamster monoclonal anti-CD11c, APC, clone N418	eBioscience	Cat#17-0114-81; RRID:AB_469345
Rat monoclonal anti-CD11b, PE-Cy7, clone M1/70	eBioscience	Cat#25-0112-82; RRID:AB_469588
Mouse monoclonal anti-CD3, clone OKT3	eBioscience	Cat#16-0037-85;RRID:AB_468855
Armenian hamster monoclonal anti-FceR1α, PE-Cy7, clone MAR-1	eBioscience	Cat#25-5898-80; RRID:AB_2573492
Rat monoclonal anti-CD45, PE-Cy7, clone 30-F11	BioLegend	Cat#103114; RRID:AB_312979
Armenian hamster monoclonal anti-CD3e, APC-Cy7, clone 145-2C11	BioLegend	Cat#100329; RRID:AB_1877171
Rat monoclonal anti-CD19, APC, clone 6D5	BioLegend	Cat#115511; RRID:AB_313646
Rat monoclonal anti-Ly6G, APC, clone 1A8	BioLegend	Cat#127613; RRID:AB_1877163
Mouse monoclonal anti-CD45.2, APC-Cy7, clone 104	BioLegend	Cat#109823; RRID:AB_830788
Rat monoclonal anti-CD4, PE-Cy7, clone GK1.5	BioLegend	Cat#100421; RRID:AB_312706
Rat monoclonal anti-CD11b, APC, clone M1/70	Millipore	Cat# MABF520
Rat monoclonal anti-IFN-γ, FITC, clone XMG1.2	BD Biosciences	Cat#562019; RRID:AB_10893998
Mouse monoclonal anti-Siglec-F, PE, clone E50-2440	BD Biosciences	Cat#562068; RRID:AB_10896143
Rat monoclonal anti-Siglec-F, APC-Cy7, clone E50-2440	BD Biosciences	Cat#565527; RRID:AB_2732831
Rat monoclonal anti-c-Kit, PE, clone ACK45	BD Biosciences	Cat#553869; RRID:AB_395103
Armenian hamster monoclonal anti-CD3e, clone 145-2C11	BD Biosciences	Cat#553058; RRID:AB_394591
Armenian hamster monoclonal anti-CD28, clone 37.51	BD Biosciences	Cat#553295; RRID:AB_394764
Mouse monoclonal anti-CD28, clone CD28.2	BD Biosciences	Cat# 555725; RRID:AB_396068
Mouse monoclonal anti-Stat6 (pY641), clone J71-773.58.11	BD Biosciences	Cat#558241; RRID:AB_647299
Mouse monoclonal anti-DRD4, clone 2B9	Millipore	Cat#MABN125; RRID:AB_10917077
Rabbit polyclonal anti-tyrosine hydroxylase	Millipore	Cat#AB152; RRID: AB_390204

REAGENT or RESOURCE	SOURCE	IDENTIFIER
Rabbit polyclonal anti-dopamine beta hydroxylase	Millipore	Cat#AB1585; RRID:AB_90805
Rabbit polyclonal anti-trimethyl-Histone H3 (Lys27)	Millipore	Cat#07-449; RRID:AB_310624
Mouse monoclonal anti-neural class III beta-tubulin, Clone Tuj1	R&D Systems	Cat#MAB1195; RRID:AB_357520
Rabbit polyclonal anti-CD4	Novus	Cat#NBP1-19371SS; RRID:AB_10011114
Rabbit polyclonal anti-vesicular acetylcholine transporter	Abcam	Cat#ab68986; RRID:AB_1143827
Rabbit polyclonal anti-DRD4	Sigma-Aldrich	Cat#SAB4500672; RRID:AB_10743979
Rabbit polyclonal anti-calcitonin gene related peptide	Sigma-Aldrich	Cat#C8198; RRID:AB_259091
Mouse monoclonal anti-β-actin	Sigma-Aldrich	Cat#A5441; RRID:AB_476744
Goat polyclonal anti-rabbit, HRP	Santa Cruz Biotechnology	Cat#sc-2004; RRID:AB_631746
Goat polyclonal anti-mouse, HRP	BD Biosciences	Cat#554002; RRID:AB_395198
Biological Samples		
Human donor lungs	International Institute for the Advancement of Medicine	https://www.iiam.org/
Chemicals, Peptides, and Recombinant Proteins		
OVA	Sigma-Aldrich	Cat#A5503
Dispase II	Sigma-Aldrich	Cat#4942078001
Red blood cell lysis buffer	Sigma-Aldrich	Cat#R7757
L-745,870 hydrochloride	Sigma-Aldrich	Cat#L131
Raclopride	Sigma-Aldrich	Cat#R121
SCH-23390 hydrochloride	Sigma-Aldrich	Cat#D054
A-412997 dihydrochloride	Sigma-Aldrich	Cat#SML0608
CAS285986-31-4	Sigma-Aldrich	Cat#573108
Epinephrine	Sigma-Aldrich	Cat#E4250
Norepinephrine	Sigma-Aldrich	Cat#A7257
Methacholine	Sigma-Aldrich	Cat#A2251
Imject alum	Thermo Fisher	Cat#77161
Dopamine	Thermo Fisher	Cat#35-485-0
RIPA buffer	Thermo Fisher	Cat#PI89900
Pierce™ Protein A/G Agarose	Thermo Fisher	Cat# 20421
Salmon sperm DNA	Thermo Fisher	Cat#15632011
DZNep	EMD Millipore	Cat# 252790-2MG
Forskolin	Tocris	Cat#1099
6-Hydroxydopamine hydrobromide	Tocris	Cat#2547
Collagenase Type 4	Worthington-Biochem	Cat#LS004188
DNase I	NEB	Cat#439807
cOmplete™proteinase inhibitor cocktail	Roche	Cat#11697498001
Proteinase K	Roche	Cat#14164600
RNase A	Qiagen	Cat#1031301
Fixable Viability Dye eFluor™ 520	eBioscience	Cat#65-0867-18

REAGENT or RESOURCE	SOURCE	IDENTIFIER
Fixable Viability Dye eFluor™ 780	eBioscience	Cat#65-0865-14
Cell Stimulation Cocktail (plus protein transport inhibitors)	eBioscience	Cat#00-4975-03
Fixation/permeabilization solution	BD Biosciences	Cat#554722
Perm/Wash™ solution	BD Biosciences	Cat#554723
Murine IL-4	BioLegend	Cat#574302
Murine IL-2	R&D Systems	Cat#402-ML-010
Murine IL-12	R&D Systems	Cat#419-ML-010
Murine IL-6	R&D Systems	Cat#406-ML-005
Murine IL-23	R&D Systems	Cat#1887-ML-010
Human IL-4	R&D Systems	Cat#204-IL-010
Human IL-2	R&D Systems	Cat#202-IL-010
Human TGF-β	R&D Systems	Cat#240-B-002
HDM	Greer Laboratories	Cat#XPB70D3A25
Critical Commercial Assays		
Naïve CD4$^+$ T cells isolation kit, mouse	Miltenyi Biotec	Cat#130-104-453
Naïve CD4$^+$ T cells isolation kit, human	Miltenyi Biotec	Cat#130-094-131
CD4$^+$ T cells isolation kit, mouse	Miltenyi Biotec	Cat#130-104-454
CD90.2 MicroBeads, mouse	Miltenyi Biotec	Cat#130-049-101
LS columns	Miltenyi Biotec	Cat#130-042-401
Lympholyte®-Mammal Cell Separation Media	Cedarlane®	Cat#CL5115
Mouse on Mouse Kit	Vector Laboratories	Cat#BMK-2202
Hematoxylin QS	Vector Laboratories	Cat#H-3404
Standard ABC kit	Vector Laboratories	Cat#PK-6100
DAB Peroxidase Substrate Kit	Vector Laboratories	Cat# SK-4100
PAS Staining Kit	Sigma-Aldrich	Cat#395B-1KT
IgE Ready-SET-Go! ELISA set	eBioscience	Cat#88-50460-88
IL-4 Ready-Set-Go! ELISA set	eBioscience	Cat#88-7044-86
IL-5 Ready-Set-Go! ELISA set	eBioscience	Cat#88-7054-88
IL-13 Ready-Set-Go! ELISA set	eBioscience	Cat#88-7137-76
Norepinephrine ELISA Kit	Abnova	Cat#89-028-610
Dopamine ELISA kit	Abnova	Cat#89-028-620
cAMP XP® Assay Kit	Cell signaling	Cat#4339S
Mouse OVA Specific IgE ELISA Kit	BioLegend	Cat#439807
CFSE Cell Division Tracker Kit	BioLegend	Cat#423801
RNeasy kit	Qiagen	Cat#74106
Superscript III Reverse Transcriptase Kit	Thermo Fisher	Cat#18080-044
PicoPure RNA isolation kit	Thermo Fisher	Cat#KIT0204
SuperScript IV VILO Master Mix	Thermo Fisher	Cat#11756050
SuperSignal™ West Pico PLUS Chemiluminescent Substrate	Thermo Fisher	Cat#34577

REAGENT or RESOURCE	SOURCE	IDENTIFIER
Deposited Data		
Raw and analyzed data	This paper	GSE137968
Full genome sequences for Mus musculus (UCSC version mm10)	UCSC	https://genome.ucsc.edu/cgi-bin/hgGateway?db=mm10
Experimental Models: Organisms/Strains		
Mouse: *Drd4*−/−: B6.129P2-Drd4<tm1Dkg>/J	The Jackson Laboratory	JAX:008084
Mouse: OT-II: B6.Cg-Tg(TcraTcrb)425Cbn/J	The Jackson Laboratory	JAX:004194
Oligonucleotides		
Primers for ChIP PCR and qPCR	(Dettman et al., 2011;Tumes et al., 2013)	See the listed, previous publications for detail
Software and Algorithms		
FlowJo Software (version 10.5.3)	FlowJo	https://www.flowjo.com/
GraphPad Prism 6	GraphPad Software	https://www.graphpad.com
ImageJ 1.49v	ImageJ	https://imagej.nih.gov
R (version 3.2.5)	The R Foundation	https://www.r-project.org/
FastQC v.0.11.2	Babraham Institute	https://www.bioinformatics.babraham.ac.uk/projects/fastqc/
TopHat (version 2.0.13)	Johns Hopkins University	https://ccb.jhu.edu/software/tophat/index.shtml
HTSeq v.0.6	(Anders et al., 2015)	https://htseq.readthedocs.io